UNIVERSITY OF CALIFORNIA, SAN DIEGO

Structural and Functional Study of Virus Protein ‘u’ from HIV-1 by Nuclear Magnetic Resonance Spectroscopy

A dissertation submitted in partial satisfaction of the requirements for the degree Doctor of Philosophy

in

Chemistry

by

Yan Wang

Committee in Charge:

Professor Stanley J. Opella, Chair
Professor John Guatelli
Professor Elizabeth A. Komives
Professor Terunaga Nakagawa
Professor Amitabha Sinha

2012

The Dissertation of Yan Wang is approved, and it is acceptable in quality and form for publication on microfilm and electronically

_____

_____

_____

_____

_____
Chair

University of California, San Diego

2012

DEDICATION

For my parents, Jinxi Wang and Qinghua Lu

who have sacrificed so much to provide the foundation

and opportunities for me to pursue my dreams.

EPIGRAPH

Whether you think you can, or you think you can't, you're right.

- Henry Ford

TABLE OF CONTENTS

.

LIST OF ABBREVIATIONS

^{1}H	Proton
^{2}H	Deuterium
^{13}C	Carbon-13
^{15}N	Nitrogen-15
^{31}P	Phosphorus-31
AMS	Ammonium sulfate
APS	Ammonium persulfate
BST-2	Bone marrow stromal antigen 2
CNBr	Cyanogen bromide
CSA	Chemical shift anisotropy
CSI	Chemical shift index
DDM	n-Dodecyl-β-D-maltoside
DHPC	1,2-dihexanoy-sn-glycero-3-phosphocholine
DMPC	1,2-dimyristoyl-sn-glycero-3-phosphocholine
DPC	Dodecylphosphocholine
DTT	Dithiothreitol
EDTA	Ethylenediamine tetracetic acid
ER	Endoplasmic reticulum
HSQC	Heteronuclear single quantum coherence
HIV	Human immunodeficiency virus
HEPES	4-(2-hydroxyethyl)-1-piperazineethanesulfonic acid

HFIP	1,1,1,3,3,3-Hexafluoro-2-propanol
IPAP	In-phase/anti-phase
IPTG	Isopropyl β-thiogalactoside
KSI	Ketosteroid isomerase
LB	Luria-Bertani
MTSL	S-(2,2,5,5-tetramethyl-2,5-dihydro-1H-pyrrol-3-1)methyl methansulfonthiate
NMR	Nuclear magnetic resonance
NOE	Nuclear Overhauser effect
PDB	Protein data bank
PISA	Polarity index slant angle
PISEMA	Polarization inversion with spin exchange at the magic angle
PRE	Paramagnetic relaxation enhancement
SDS	Sodium dodecyl sulfate
SDS-PAGE	Sodium dodecyl sulfate-polyacrylamide gel electrophoresis
RMSD	Root mean squared deviation
TEMED	N,N,N',N'-tetramethylenediamine
TFE	2,2,2-Trifluoroethanol
TM	Transmembrane
TOCSY	Total correlation spectroscopy
Vpu	Virus Protein 'u'
WT	Wild type

LIST OF FIGURES

ACKNOWLEDGEMENT

First and foremost, I would like to my thesis advisor, Professor Stanley Opella for giving me the opportunity to conduct cutting edge research in his laboratory. None of my accomplishment would be possible without his guidance, scrutiny, and encouragement. He has provided a research environment that is both intellectually challenging and uplifting, and I have become a truly independent scientist because of that. I would like to give many thanks to members of the Opella research group. They have been an integral part of my graduate career and given me support both professionally and personally. Special acknowledgement must be given to Dr. Sang Ho Park for sharing his expertise and insights that have helped me tremendously since the beginning. I would like to thank Hua Zhang for helping me on the Vpu project while making great progress with this very challenging protein on her own effort. Acquisition of solid-state NMR data would not be possible without the patient assistance of Dr. Chris Grant and Dr. Albert Wu at the Center for NMR Spectroscopy and Imaging of Proteins, "The Bubble". Likewise, the assistance of Dr. Xuemei Huang was indispensable in the collection of the solution NMR data. I would like to thank Dr. Henry Nothnagel for sharing his expertise on the paramagnetic spin label and Dr. Ye Tian for his help on the structure and docking calculations.

I would like to thank Prof. John Guatelli and Dr. Mark Skasko at UCSD School of Medicine for the collaboration on Vpu-BST-2 project. Dr. Skasko has provided the DNA for many of the constructs in the project, and I gained tremendous amount of knowledge in the biological aspect of study from this experience. Even

though we are in very different disciplines, their willingness to share and listen has made the whole process a wonderful experience. I also would like to thank the other members of my thesis committee, Prof. Komives, Prof. Nakagawa, and Prof. Sinha, for their continuing guidance and support.

I would like to thank Prof. Mary Roberts at Boston College who was my undergraduate research advisor and mentor. She opened the door to my research career and gave me the confidence to pursue a doctorate. I would also like to thank Prof. Yaotang Wu and Prof. Jerry Ackerman at Massachusetts General Hospital for introducing me to the fascinating world of NMR and MRI.

Chapter 3, in part, is currently being prepared for submission for publication of the material. Wang, Y., Park, S.H., and Opella, S.J. The dissertation author was the primary investigator and author of this material.

Chapter 4, in part, is a reprint of the material as it appears in the Journal of Biological Chemistry 2011. Skasko, M., Wang, Y., Tian, Y., Tokarev, A., Munguia, J., Ruiz, A., Stephens, E.B., Opella, S.J., and Guatelli, J. The dissertation autor was the co-first author of this paper.

CURRICULUM VITA

2004 Bachelor of Science, Biochemistry, Boston College

2008 Master of Science, Chemistry, University of California, San Diego

2012 Doctor of Philosophy, Chemistry, University of California, San Diego

PUBLICATIONS

Skasko, M.,* Wang, Y.,* Tian, Y., Tokarev, A., Munguia, J., Ruiz, A., Stephens, E.B., Opella, S.J., and Guatelli, J. HIV-1 Vpu antagonizes the innate restriction factor BST-2 via lipid embedded helix-helix interactions. *Journal of Biological Chemistry*. 2011. In-press. * Contributed equally

Son, W.S., Park, S.H., Nothnagel, H.J., Lu, G.J., Wang, Y., Zhang, H., Cook, G.A., Howell, S.C., and Opella, S.J. 'q-Titration' of long-chain and short-chain lipids differentiates between structured and mobile residues of membrane proteins studied in bicelles by solution NMR spectroscopy. J. Magn. Reson. 2011. In-press.

Cook, G.A., Zhang, H., Park, S.H., Wang, Y., and Opella, S.J. Comparative NMR studies demonstrate profound differences between two viroporins: p7 of HCV and Vpu of HIV-1. *Biochimica et Biophysica Acta – Biomembranes*. 2011, 1808(2):554-60.

Wang, Y., Spiller, M., and Caravan, P. Evidence for weak protein binding of commercial extracellular gadolinium contrast agents. *Magn Reson Med*. 2010, 63(3):609-16.

Rodionov, D.A., Kurnasov, O.V., Stec, B., Wang, Y., Roberts, M.F., and Osterman, A.L. Genomic identification and in vitro reconstitution of a complete biosynthetic pathway for the osmolyte di-myo-inositol-phosphate. *Proc Natl Acad Sci USA*. 2007, 104(11):4279-84.

Neelon, K., Wang, Y., Stec, B., Roberts, M.F. Probing the structure of Archaeoglobus fulgidus inositol-1-phosphate-synthase with site-directed mutants. *J Biol Chem*. 2005 280(12):11475-82.

Wu, Y., Ackerman, J.L., Chesler, D.A., Graham, L., Wang, Y., Glimcher, M.J. Density of organic matrix of native mineralized bone measured by water and fat suppressed proton projection MRI. *Magn Reson Med*. 2003, 50(1):59-68.

ABSTRACT OF THE DISSERTATION

Structural and Functional Study of Virus Protein ‘u’ from HIV-1

by Nuclear Magnetic Resonance Spectroscopy

by

Yan Wang

Doctor of Philosophy in Chemistry

University of California, San Diego, 2012

Professor Stanley J. Opella, Chair

Virus protein ‘u’ (Vpu) is one of the accessory proteins expressed by the HIV-1 genome. It is a type I integral phosphoprotein which contains a single-helical transmembrane (TM) domain and an amphipathic cytoplasmic domain. In its oligomeric form, the transmembrane domain is responsible for the ion channel activity of Vpu, and the domain itself is the main contributor in the antagonistic function against BST-2, a host cell viral restriction factor. The cytoplasmic domain is responsible for the binding of CD4 receptors at the endoplasmic reticulum (ER) and recruiting other protein complexes that ultimately leads to the CD4 degradation through the ubiquitin-proteasome degradation pathway. In order to structurally characterize this protein by NMR, a lipid environment in the form of either micelle or

bicelle was used for the proper solubilization and folding of the protein. Solution NMR was used as a method to quickly examine the stability of the protein within micelles and to identify the secondary structure regions, while solid-state NMR gave helical tilt and rotation information as well as the orientation restraints of individual amide bonds for a protein embedded in a bilayer environment. In this thesis, structural features of Vpu based on NMR results of wildtype and various truncated/mutant forms of the protein are presented. A single site mutation on the TM that enables the inter-conversion of structure and functionality between Vpu and M2, a structural analogue from Influenza A virus, will be discussed. The last section will describe the collaborative effort of examining the protein-protein interaction between Vpu and BST-2 using a combination of spectroscopic, biological, and computational approaches. Residues involved in the interaction between the two proteins' TM domains were identified in solution NMR experiments while the helical tilt angles and interaction faces were determined by solid-state NMR. A model of the complex is presented and shows remarkable agreement with the combination of NMR data, biological results, and computational simulation.

Chapter 1. General Introduction

1.1 Introduction to Membrane Proteins

Membrane proteins serve vital and diverse functions in cell biology and can account for up to one third of the prokaryotic and eukaryotic genomes. They can serve as membrane receptors as the 7-transmembrane G-protein coupled receptors (GPCRs), cell adhesion molecules such as integrin, transporters such as the potassium channel, and membrane enzymes such as the phosphatsase and tensin homolog (PTEN). Structurally, they can be in the form of α-helix or β-sheets. The first atomic resolution structure was determined in 1985 for the photosynthetic reaction center of *Rhodopseudomonas viridis* (Deisenofer 1985). Since then, membrane proteins have remained as a big challenge to structural biology. There are various reasons for this challenge, but arguably the most crucial one is the requirement of a lipid environment for the proper folding and function of the membrane protein. Achieving atomic resolution structures requires the application of biophysical method on proteins removed from its native environment and compacted at a high concentration. This inevitably leads to problems with aggregation, mis-folding, and precipitation because of the hydrophobic nature of membrane proteins.

In order to circumvent these problems, artificial lipids and detergents have been commonly used to mimic the membrane environment in order to facilitate the solubilization and proper folding of proteins. These “artificial membranes” are composed of lipids or detergents that contain a hydrophobic hydrocarbon chain and a water-soluble head group. There are various types of lipids and detergents that can

have different lengths of hydrocarbon chain, and the head-groups can be in polar, anionic, cationic, or zwitterion forms. They also behave differently in solution depending on their identity and composition. Lipids or detergents such as DHPC or SDS spontaneously form micelles in solution as the lowest energy form assembly, whereas long chain lipids such as DMPC can exist as liposome suspensions in pure water. When lipids with long carbon chains (generally greater than 12) mix with short chain lipids or detergents (Whiles 2002), they can form an assembly called bicelles. Bicelles can be described as a disc shaped conglomerate with the long chain lipids making up the bulk and the short chain lipids or detergents capping the rim, though this view is still currently open for debate. Another form of membrane mimic is a liposome which is composed of only long chain lipids, and it is a hollowed sphere whose surface is made of a lipid bilayer. As it will be discussed in detail in the spectroscopy section of the introduction, the important feature regarding various forms of assemblies is the time scale of the motion associated with them. In other words, as the size of the assembly increases, the motion becomes slower, and that will directly affect the NMR data collected on proteins embedded in these environment.

In addition to finding a suitable lipid environment, optimization of protein expression and purification also plays a crucial role in tackling the challenges of characterizing membrane proteins. When expressing a large amount of membrane proteins to the cell surface in heterologous expression, the cell growth can be dramatically impaired by the proteins disrupting the cell membrane or forming ion-channels that cause cell lysis. One strategy to circumvent the problem is to express the

membrane protein together with a fusion partner which can not be properly folded in the cells and thus is expressed into inactive inclusion body. This approach significantly lowers the toxic effect for over-expressing membrane proteins. During purification procedures, proteins can not be solublized in aqueous environment alone, so denaturant, lipids/detergents, or organic solvents are need throughout the steps, especially during chromatographic methods. Therefore, a lot of effort is spent on optimization to find the proper condition so that the proteins do not become aggregated or mis-folded during the procedure.

1.2 Solution and Solid-State NMR Techniques for Studying Membrane Proteins

When a membrane protein is incorporated into a micelle with no presence of aggregate, the complex is water-soluble and behaves as a soluble protein in terms of its fast rotational motion. It has been estimated that an average micelle complex is similar to a 15-20 kD protein based on the measurement of rotational correlation time (Krueger-Koplin 2004). Therefore, to a certain extent, standard solution NMR techniques for soluble protein characterization can therefore be applied to membrane proteins in micelle. Isotopically labeled (^{15}N and/or ^{13}C) protein is often a requirement to properly resolve the resonance signals from the backbone and side-chains. The first experiment used typically for evaluating the sample is ^{1}H-^{15}N-HSQC which, through the scalar coupling, correlates the proton signal to the nitrogen it is boned to. A HSQC spectrum shows all of the backbone and side chain amide signals. Once a well-solved spectrum is obtained, a series of triple resonance experiments are applied to ^{15}N and

^{13}C lableled protein to assign the resonances frequencies to the atoms in specific amino acid residues. A typical experiment is the HNCA which correlates the backbone amide resonance with the Cα signals of the same and previous residues. This correlation can then be used to trace or "walk" along the backbone. Additional triple-resonance experiments such as the HNCOCA can be performed to resolve ambiguities of the assignment due to inadequate resolution or low signal to noise ratio. In addition, selectively labeled protein in which only one or a few amino acid(s) are isotopically labeled can be very helpful in the assignment process. Side chain signals can be visualized and assigned using a combination of TOCSY and NOE experiments. These techniques and methodologies mentioned above are well established, and detailed descriptions can be found in many literatures (Leopold 1994, Whitehead 1997).

The assignment procedure on membrane proteins is relatively straightforward for the protein backbone but can be very difficult when dealing with the side-chains. If the membrane proteins only contain hydrophobic helices which is the case for most proteins studied by the group, the chemical shift dispersion will be small due to similar secondary structure environment and an abundance of hydrophobic residues such as leucine and isoleucine. This will result in a greater tendency for overlapping peaks arising from degenerate chemical shift values. This is a relatively minor issue for backbone amide resonances but becomes significant when resolving carbon signals. Side chains correlation experiments that extend beyond the Cβ region can also be problematic because poor signal intensity due to the long mixing time required for complete magnetization transfer.

Typical solution NMR based structure restraints involve inter-nuclei distances derived from NOE based experiments. While they provide valuable information for structure calculation, they are difficult to apply to membrane proteins, especially for determining with tertiary fold. There are two main issues in NOE measurement, and the first one is the large effective size of the protein-micelle complex. As described in the beginning part of this section, the complex behaves essentially as a large protein. As the molecular weight increases, so does the rotation correlation time (τ_c), and this leads to a decrease in T_2 relaxation time as $T_2 \sim 1/\tau_c$ (Schramm 1983). This results in the faster decay of NMR signal and broadening of the peak linewidth. Another contribution to the decrease in resolution due to fast T_2 relaxation is the dipole-dipole (DD) relaxation from the near by nuclei. In the case of membrane protein, these nuclei are protons from the hydrocarbon chains of the lipids. DD relaxation is negligible for small molecules that tumbles very fast, but for large ones that tumbles slowly, the effect is much more significant. There are a few ways to alleviate the problems described above. For example, one can run the experiment at higher temperature to increase the correlation time of the complex, and deuterated lipids can be used to reduce the dipolar relaxation factor. However, the former may decrease the stability of the protein sample, and the latter is simply very costly. When performing NOE experiments to obtain long-distance restraints which are crucial in determining the tertiary folds, extended pulse sequences with long mixing times are required. NOE intensities are difficult to measure because during longer NOE mixing times, magnetization decay occurs simultaneously with through space magnetization transfer,

thus reducing the signal to noise ratio. Therefore, alternative approaches are needed in order to obtain the structural restraints.

One effective approach is measuring the dipolar coupling which is a through space interaction between two spins, and this interaction is normally averaged to zero under the isotropic condition in solution NMR. However, it can be regained by introducing an agent in the solution that forces the protein to have a slight preferential orientation. The agent is often called an alignment medium, and typical examples include polyacrylamide gel, bicelles, liquid crystals, and phages. They function by introducing a steric or electrostatic hindrance to the protein. Since the proteins are only partially aligned as opposed to the full alignment condition in solid-state, the term "residual" is added on. The coupling measured using this technique is thus termed residual dipolar coupling (RDC). The observed RDC value (D_{AB}) in solution between two nuclei A and B can be described by the following equation (Lipsitz 2004)

$$D_{AB}(\theta,\phi) = A_a^{AB}\left\{(3\cos^2\theta - 1) + \frac{3}{2}R(\sin^2\theta\cos 2\phi)\right\}$$

where

$$A_a^{AB} = -\left(\frac{\mu_0 h}{16\pi^3}\right)S\gamma_A\gamma_B\left\langle r_{AB}^{-3}\right\rangle A_a$$

A_a is the principle axis component of the molecular alignment tensor. Supposing there is a vector going through the nuclei A and B, θ is the angle between the vector and the z-axis of the alignment tensor, and Φ is angle between x-y plane project of the vector and the x-axis of the vector. μ_0 is the vacuum permeability constant, and *h* is Planck's constant. γ is the gyromagnetic ratio of the nucleus, and r is internuclear distance. As

the equation indicates, RDC is dependent on the orientation of the vector connecting the two nuclei with respect to the magnetic field through the molecular alignment tensor. Therefore, the orientation information can be extracted if one is to measure RDC for a bonded system such as the amide of the protein backbone. Experimentally, RDC can be measured by taking the difference of coupling value of a bond under isotropic and anisotropic conditions. The pulse sequences involves HSQC type correlation experiment but with decoupling turned off to enable the measurement of the splitting. The contribution from RDC to the peak splitting can be positive or negative depending on the orientation of the bond.

The advantage in RDC is that it is a direct experimental observation without any long mixing time, so the issue associating with the fast signal decays of large molecular weight of the protein or protein-micelle complex would not be a major impedance in the measurement. In practice, larger proteins would still have the added challenge in the crowding of peaks and thus in extracting the chemical shift values. Therefore, as long as one is able to obtain a well-resolved HSQC spectrum of the protein, this technique can be applied to that protein. RDC provides valuable information that can be applied directly towards the structure calculation. First of all, RDC is an accurate and clear indicator of secondary structure, especially for an alpha helix. With an ideal helix conformation, the amide bond is distributed within a cone shape. The resulting RDC values for the backbone amides in a helix display a periodicity that can be fitted by a sinusoidal curve termed a “Dipolar Wave” (Mesleh 2003). An example of the dipolar wave is shown in Fig 1.1. The figure plots the

residual dipolar coupling values against their corresponding residue numbers as series of dots, and data are fitted with a wave using a previously published formula for an ideal helix (Nevzorov 2004).

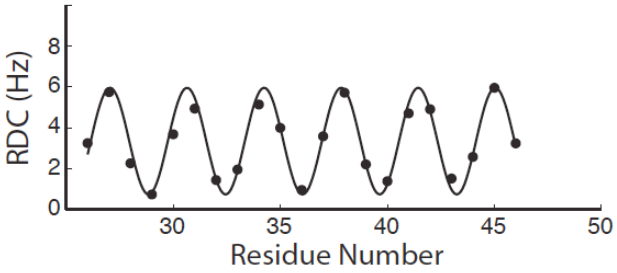

Figure 1.1: Example of dipolar wave. The dots represent correlations between backbone amide RDC values and their corresponding residues. The sinusoidal wave is fitting on the dots and a perfectly fitted wave is an indication that the residue are within an ideal helical secondary structure.

If the residues are within a well-defined single helix, a single dipolar wave shown can be fitted onto the experimental RDC data. Likewise, several of such curves can be fitted if the protein contains more than one helix. In addition, any deviations from an ideal helix such as a kink can be shown through a discontinuity in the phase and some times magnitude of the dipolar wave. Therefore, the regions of secondary structure can be clearly identified, and during structure calculation, angular constraints can be applied to such regions to conform the backbone. The residues not adapting a secondary structure topology such as the ones in a loop or coiled region will generally yield two characteristic RDC patterns. In one case when the protein region is unstructured and very flexible, structural mobility prevents the residues from being in an aligned state thus causeing the RDC values to be around zero. In the other case, if

the region is unstructured but still rigid, the RDC will be randomly distributed instead of in a periodic pattern.

In order to determine the tertiary fold for monomeric protein or quaternary fold of an oligomeric protein, long distance constraints are needed, but these are often the hardest to obtain. With RDC values, this information can be extracted from the difference of how each discrete secondary structure region is positioned with respect to the alignment tensor. In other words, the 3-dimensional backbone structure can be represented in terms of how the secondary structure regions orient with respect to one and another as building blocks that are connected by loops and coils. Implementing such an approach into practice, however, can be difficult primarily because of the degeneracy of the RDC values. In other words, two or more different structural solutions can fit the same set of RDC values. Certain solutions can be eliminated by enforcing the restraints of the physically allowed dihedral angles for peptides. The number of possible solutions can be further narrowed down in the case of transmembrane proteins because the presence of lipid does not allow certain conformations to be energetically favorable. In most cases, however, a second or even more alignment media that gives a uniquely different alignment tensor is needed in order to solve the degeneracy problem if RDCs are the only structural restraint. This is an area of active development in the field of protein structure calculation, and there are a number of softwares (Mukhopadhyay 2009) that take in a multiple sets of RDC, and perform alignment tensor estimation and provide novel protein folding and dynamics information.

Another technique for obtaining long distance information is the measurement of paramagnetic relaxation enhancement (PRE). PRE arises from the dipolar interaction between an unpaired electron and a nucleus. Like the NOE, its magnitude is proportional to r^6 where r is the distance between the electron and nucleus. Because of the large magnetic moment of the electron, the effect from PRE can reach much larger distances (up to 35Å) when compared to the 6Å range of NOE. It is therefore a valuable technique for deriving rough intramolecular or intermolecular distances that are too long for other methods to measure. As evidence of its sensitivity and versatility, PRE has been used for the analyses of protein structure (for soluble and membrane types), protein-protein interaction, protein-nucleic acid interaction, and conformational flexibility in unstructured proteins (Clore 2007). Another advantage of PRE is that the preliminary measurement can be done with only basic 2D experiments such as ^{1}H-^{15}N HSQC without employing elaborate pulses sequences or long mixing times. In this thesis, PRE will be discussed in terms of two distinct applications. The first one is using paramagnetic relaxation agents to qualitatively map the protein's exposure to solvent or lipids. Manganese Ethylenediaminetetraacetic acid (Mn-EDTA) is a commonly used water soluble metal-chelate which utilizes the paramagnetic property of the Mn atom to selectively increase the relaxation of nuclei not shielded by the hydrophobic environment of a lipid or detergent micelle. This will result in the selective broadening of resonance peaks and thus decrease in peak intensities. This technique can be used to complement and confirm the information gathered by D_2O exchange experiments in which the exchange of protons for deuterons is prevented by

the hydrophobic micelle protection. In certain cases, Mn-EDTA PRE can even provide more accurate information. Because of protein dynamics and the potential for ion-channel formation in certain membrane proteins, water can still penetrate the hydrophobic core of micelle whereas the bulk and electrostatic charge of Mn-EDTA prevent it from entering the micelle interior. Paramagnetic agents can also be added to lipids/detergents to map the residues located within the hydrophobic core. Examples of such agents are doxyl-stearic acids where a 4,4-dimehyl-3-oxazolidinyloxy (doxyl) group is attached to one of the carbons on the hydrocarbon chain of a fatty acid. This compound can be incorporated into the micelle because of its amphipathic nature and used to selectively broaden the peaks that correspond to residues positioned within the hydrophobic core of the micelle. Another usage for the PRE is for providing structural restraints for membrane proteins, and it involves attaching a relaxation agent to a residue on the protein. A commonly used agent is (2,2,5,5-tetramethyl-2,5-dihydro-1H-pyrrol-3-yl)methyl methanesulfonothioate (MTSL) which contains a paramagnetic nitroxide group and can be covalently attached to the side-chain of cysteine through a disulfide bond. The cysteine residue can be part of the natural protein sequence or introduced by site-directed mutagenesis. Typically, the effective radius of MTSL is between 10-25 Å, and atoms within 10 Å of the paramagnetic group will have their resonances broaden beyond detection while those beyond 25 Å are not significantly perturbed. The valuable information comes from affected residues which are far away from the cysteine in the primary structure. In terms of membrane protein in this study, the distances between the helices are valuable information for either determining the

tertiary fold of a single protein or identifying protein-protein interactions. Because of the r^6 dependence of PRE, distance information can be quantitatively extracted by isolating the nuclei relaxation increase solely due to the paramagnetic center. Peak intensity and linewidth of resonances in the presence the MTSL are compared to those either in the presence of a diamagnetic analogue of MTSL or chemically reduced MTSL which loses its paramagnetic property. A commonly used reducing agent is ascorbic acid. The ratio of the peaks intensities with and without the paramagnetic contributions can be used to estimate the distance from the lone electron to the corresponding nuclei by using formulas described by Battiste and Wagner (Battiste 2000).

The description thus far has been focused on solution NMR techniques for membrane proteins in a micelle environment. As mentioned previously, the isotropic nature and the motional time scale of the complex allows for the application of solution NMR techniques. This also extends to proteins in isotropic bicelles which contain a small amount of long-chain lipids and behave essentially the same as micelles. However, when the protein is incorporated into larger membrane mimicking systems such as aligned bicelles or liposomes, the most of the solution NMR methods become ineffective because of additional components that come into play. One of the most important components is dipolar coupling (DC). As introduced in the earlier paragraphs on RDC, DC is a through space interaction between spins and has an orientation dependence. When applying solution technique to a solid-state sample, the signals are broadened beyond detection due to the relaxation mechanism introduced by

DC. When using solid-state NMR, signals can be observed by applying high power pulses and large sweep width, but the line-widths are generally still too broad to give any resolution and thus are of very little use for structural characterization. There are a number of established strategies in solid-state NMR to gain the resolution and sensitivity of the signals necessary for biomolecular studies. One such strategy is magic angle spinning (MAS) which involves spinning the sample at high speed within a rotor at the 'magic angle' (54.7°) with respect to the magnetic field to remove the dipolar coupling interaction and average the chemical shift tensors. Details regarding MAS background and application on membrane proteins will not be discussed in detail here. They can be found in a number of informative reviews (McDermott 2009, Alia, 2009). The primary solid-state technique used for this thesis project involves magnetically oriented samples (OS) and has several major distinctions from MAS in terms of hardware and pulse sequence components.

As mentioned in the description in section 1.1, because of their intrinsic magnetic susceptibility, bicelles can spontaneously orient themselves when placed within magnetic field such that their normal is perpendicular to the axis of the field. When proteins are incorporated into the bicelles, they also become oriented with respect to the external field as part of the complex, and this is referred as OS. Solid-state NMR (ssNMR) application on these samples requires the development of both probe and pulse sequence designs. OS ssNMR probes need to have high sensitivity and can tolerate high power radio frequency input while minimizing sample heating. The probe development is conducted in house at the Center for NMR Spectroscopy

and Imaging of Proteins at UCSD. One of the most important hardware components of any NMR probe is the receiver coil, and the two most commonly used coil designs used in this thesis study are Modified Alderman-Grant Coil (MAGC) and strip-shield (Grant 2009, Wu 2009). In terms of pulse programs, the two most frequently used pulse programs in this study are one dimensional (1D) chemical shift and two dimensional (2D) chemical shift – dipolar coupling correlation experiments. The 1D experiment involves displaying the anisotropic chemical shifts of ^{15}N nuclei, and the signal to noise ratio (S/N) is enhanced through cross polarization (CP) between ^{1}H and ^{15}N where ^{1}H is the much more abundant nuclei (Muller 1974). Chemical shift values will be dependent on the chemical shielding tensor, but they are much more simplified compared to samples with no preferential alignment, because they only occupy only a certain section of the maximum possible range of chemical shift values. However, the values still have an orientation dependence due their anisotropic nature. With the added rotational motion of the bicelle and the internal motion of the protein, the result is that each nucleus gives one peak with the line-width down to 0.5ppm in the most optimized sample (Park 2010).

The 2D experiment aims to resolve the degeneracy in the 1D spectrum through the addition of the dipolar coupling dimension for the amide bonds. The pulse program involves an initial CP transfer from proton to nitrogen followed by an evolution of nitrogen spins through dipolar coupling interaction while the protons are decoupled. Finally, the free induction decay is acquired on the nitrogen dimension. A detailed description of the specific pulse sequence used in the study can be found in

the article by Nevzorov and coworkers (Nevzorov 2003). The result of the experiment correlates the chemical shift value of a nitrogen nucleus to the dipolar coupling value of the amide bond which it is part of. Because both dimensions have orientation dependence, the spectrum carries an abundance of structural information. For helical proteins, one of the most significant and visually intuitive properties of the 2D spectrum is the wheel pattern placement of the resonances. As mentioned in the section on RDC, the arrangement of amide bonds leads to the periodic pattern of the dipolar coupling values, termed dipolar wave. By the same principle, the chemical shift (CS) values will also have periodic pattern, though it is important to note that CS value are also affected by the local fluctuating electron environment. As a result, they can not be fitted nicely with a sinusoidal wave as in the case of DC. Nevertheless, the deviation is small enough so that the pattern of the cross peaks in the 2D spectrum can be roughly fitted with an ellipse/circle, and the fitting is termed as polarity index slant angle (PISA) wheel (Marassi 2000). To generate the PISA wheel, the CS and DC values are calculated based on the relationship between the molecular frame and the external magnetic field. Details of the calculation can be found in the work by Nevzorov and coworkers (Nevzorov 2003). Structural information regarding the tilt angle of the helix within the bilayer can be extracted by fitting the PISA wheel to the experimental data since the wheel pattern changes with respect to the tilt angle. Multiple PISA wheels can fitted onto the spectrum if there is more than one distinctive helix in the protein. In order to extract the information for structure calculation, resonances need to be assigned, and there are a number of strategies for doing so. One

can selectively label the protein with ^{15}N amino acid(s) and compare the spectrum with the uniformly labeled protein. Because the resonances are in a wheel pattern that is similar to a helical wheel representation of the residues, one can extract the sequence assignment of the selective labeled residues by comparing the relative positions on the wheel without having to use additional correlation experiment. With the abundance of hydrophobic residues such as leucine, isoleucine and valine residues within the membrane proteins, typically, 2-3 selectively labeled samples can produce over 60% of all assignment. Another strategy is using D_2O exchange which is an approach similar to solution NMR. The sample can be hydrated with an environment contains >90% D_2O, and the residues not protected by the lipid bilayer will be absent from the spectrum due to the proton-deuterium exchange. This is a relatively quick method for assigning the peaks that come from the terminal regions of the protein.

1.3 Biological Significance of Vpu

There is a class of proteins expressed by the HIV-1 genome called accessory proteins that play a variety of role in facilitating the viral replication cycle. The genome construction is shown in Fig 1.2A, and nef, vif, vpr, and vpu are the accessory genes. The vpu gene encodes an approximately 80 amino acids type I transmembrane phospho-protein. It is found in HIV-1 and certain types of SIV but not in HIV-2, and the topology features are illustrated by the cartoon shown in Fig1.2B. The protein contains a N-terminal single helical transmembrane domain and a cytoplasmic domain of two amphipathic helices connected by a flexible loop. The loop has a conserved

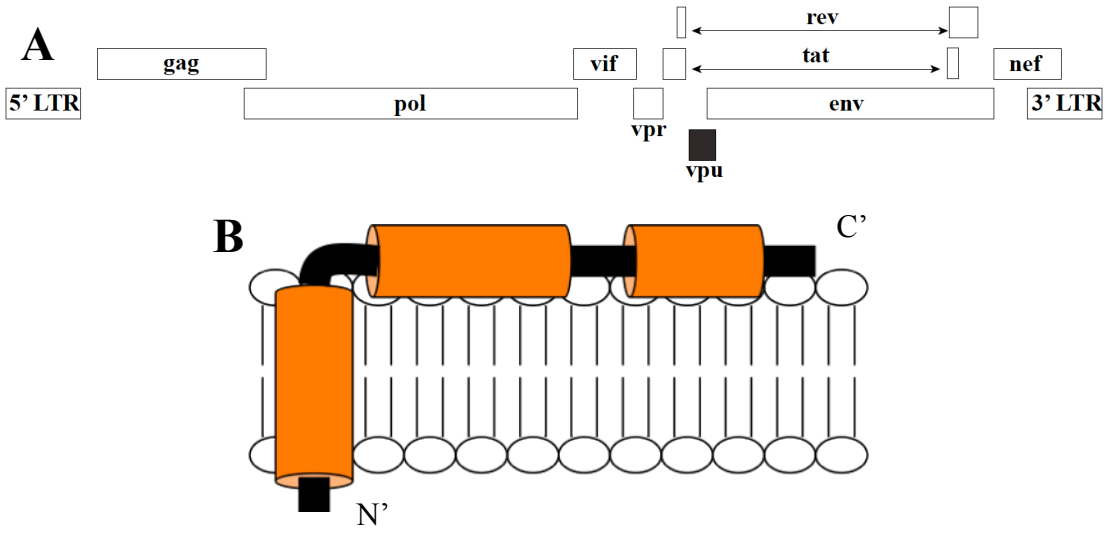

Figure 1.2: Schematic diagrams of the HIV-1 genome and Vpu. A) HIV-1 genome showing the various gene components. LTR stands for long terminal repeat, and the vpu gene is colored in black. B) Cartoon diagram showing the important features of Vpu. The helical regions are represented by orange cylinders, and the terminal and loop regions are shown as black lines. The helix on the N-terminal region is the transmebrane domain that inserts into the lipid membrane while the two C-terminal helices are amphipathic and reside on the membrane surface.

sequence of DSGNES where the serines are phosphorylated during post-translational modification. Vpu has two major functions. One is the down-regulation of CD4 receptors through the ubiquitin ligase-proteasome degradation pathway. While CD4 is important for the entry of the HIV-1 into the host cell, it has detrimental effects on the proper replication and infection of the virus. During the endoplasmic reticulum (ER) localization stage, CD4 can bind to gp160, a precursor for the proteins that are important for the proper packaging of the viral envelope. In addition, the expression of CD4 to the cell surface can promote superinfection which hinders the proper viral release (Wildum 2006). Vpu counteracts CD4 by binding to it in the ER and recruiting the $SCF^{\beta\text{-}TrCP}$ E3 ubiquitin ligase through the phosphorylated serine motif. This subsequently leads to the polyubiquitination of the CD4 and its degradation through the endoplasmic reticulum associated protein degradation (ERAD) pathway, and Vpu somehow manages to escape the degradation itself (Dube 2010). While the details of the mechanism are still being investigated, the protein-protein binding interaction and the recruitment various complexes for degradation have been extensively characterized. The other major function of Vpu is the facilitation of the mature viron release from the host cell membrane surface. It was long known that in the absence of Vpu, virus particles aggregate at cell surface during the budding process, but the mechanism of the action was not clear. In 2008, two groups have independently discovered that BST-2/HM1.24/CD317 is the restriction factor protein that prevents the release of virions, and Vpu counteracts the function of BST-2 (Van Damme 2008, Neil 2008). BST-2 is an interferon-α induced type II transmembrane protein that is

down-regulated from the cell surface with the expression of Vpu. It contains a single transmebrane helix, a coiled-coil region and a C-terminal glycophosphatidylinositol (GPI) anchor that is added during post-translational modification. Data have supported the notion that BST-2 restricts the release of virions by "tethering" itself between the host cell membrane and membrane envelope of the virus and between the viral membranes. Therefore, BST-2 has the nickname of "tetherin". Studies have shown the functional BST-2 is a dimer (Perez-Caballero 2009), and mutational analyses have placed the regions crucial for the antagonism BST-2 by Vpu to their transmembrane domains (McNatt 2009). The exact mechanism is, so far, relatively unknown. It is reasonable to expect Vpu uses the same ERAD pathway as in the case of CD4 down-regulation to remove BST-2, but the studies so far have not been conclusive. There is also an unanswered question on whether Vpu removes BST-2 directly from the cell surface or prior to that such as in the ER. Therefore, it is important as a first step to see whether the two proteins interact with each other directly, and if so, to elucidate the specific residues involved in this interaction in order to provide a molecular basis for the antagonism.

Chapter 2. Structural Characterization of Vpu in micelle and bicelle

2.1 Introduction

Since the discovery of Vpu protein in 1988 by Cohen and coworkers (Cohen 1988), there have been continuous studies on its biological functions. The research focuses on its functions of CD4 down-regulation and the facilitation of virus release as described in the previous chapter. Significant progress has been made to explain the mechanisms and interactions involved functions, but many details are still not clear and far from consensus. Structures of Vpu would be invaluable for setting a good foundation to understand the behavior of this protein and developing drugs to inhibit its activity. The high resolution structure information has not come out until more recently as the first backbone structure of Vpu TM domain has been solved using a combination of solution and solid-state NMR (mechanically aligned) in 2003 by Park and coworkers (Park 2003). The same group also later solved the backbone TM structure of wildtype as well as an A18H mutant in magnetically aligned bicelle (Park 2007). The structure of the cytoplasmic (cyto) domain was determined first in soluble state in 1997 (Willbold 1997) and then in micelle complex in 2009 (Wittlich 2009) by solution NMR. The results on the TM show that the helix spans from residues 8 to 25 in both micelle and bicelle. Interestingly, there is a kink observed in micelle and mechanically aligned bilayer but not present in magnetically aligned bicelle, and the kink occurs at residue 15 and is approximately 12°. When the TM construct is incorporated into artificial membrane environment, it exhibits ion channel activity to non-specific cations. The cyto domain structure shows two short amphipathic helices

of about 10 and 7 residues, and the connecting loop region of about 13 residues is highly flexible. In addition, it is concluded that even the presence of lipid micelle, the cyto domain has a high degree of structural flexibility. There are still numerous unanswered questions regarding the structures of Vpu. One of them is whether there is any structural dependency between TM and cyto domains. The other is regarding the effect of micelle and bicelle on the behavior of various constructs of Vpu. Moreover, response to potential antiviral drugs should be studied in order to map the protein-drug interaction.

2.2 Material and Methods

Plasmid constructs for Vpu-full length, cytoplasmic (cyto) and transmembrane (TM) have been previously described (Ma 2002, Park 2003). In an effort to lower the toxic effects of membrane proteins, the gene of interest was expressed together with a partner (ketosteroid isomerase or ΔTrp LE) as a fusion protein in order to drive the expression into inclusion bodies. pHMMa plasmid was obtained from the laboratory of Peter Kim at Massachusetts Institute of Technology (Staley 1994). The plasmid pET31b(+) was purchased from Invitrogen. Oligonucleotides were purchased from Integrated DNA Technologies, Inc. Site-directed mutagenesis was performed using Quik Change Lightening Mutagenesis Kit (Agilent Technologies). Polymerase chain reactions (PCR) were done on a PCR Sprint Temperature Cycling System (Thermo Electron Corporation). Plamids were transformed into OverExpress C41 (DE3) competent cells (Lucigen). Cells were grown in either in LB medium for unlabeled

protein production or M9 minimum medium for isotopically labeled protein. For labeled growth, M9 medium is supplement either with ^{15}N ammonium sulfate (AMS) and/or ^{13}C glucose for uniformly labeled protein or with ^{15}N amino acid(s) for selectively labeled protein. ^{15}N AMS, ^{13}C glucose and amino acids were purchased from Cambridge Isotope Laboratories, Inc. Cell growth was conducted at 37°C with continuous shaking at 250rpm, and protein expression was induced with a final concentration of 1mM isopropyl β-D-1-thiogalactopyranoside (IPTG) / liter of medium.

Unless stated otherwise, the purification for all constructs follow the steps described below. Cells were lysed using a combination of lysozyme (Sigma) and mechanical sonication. Fusion protein was purified by Ni-NTA Superflow resin (Qiagen) using guanidine hydrochloride (Gdn-HCl) or SDS as solubilizing agent for the inclusion bodies. Protein was then dissolved in 70% formic acid (Sigma) and incubated with excess amount of cyanogen bromide (CnBr) at room temperature to cleave the fusion protein at methionine residues which had been introduced between the constructs. It should be noted that the natural methionine residues in the Vpu constructs have been mutated to leucines. The cleaved protein products were further purified by HPCL on a C4 reverse phase column for the full-lengths constructs or C18 for cytoplasmic constructs. The yield varies from batch to batch, but the average is around 2mg/liter of culture for full-lengths and 5mg/liter of culture for cytoplasmic constructs.

Lipids were purchased from Avanti Polar Lipis, Inc. Micelle samples are prepared by dissolving protein in 100-150mM 1,2-dihexanyl-sn-glycero-3-phosphocholine (DHPC) with 10% deuterium oxide (D_2O), and pH was adjusted by either adding stock solution of sodium hydroxide or hydrochloric acid. Bicelle sample is prepared by first dissolving lyophilized protein powder in aqueous DHPC micelle and then adding it to 20mg of DMPC powder. The final lipid molar ratio is 3.2:1 DMPC:DHPC, and the lipid content is 15% (w/v). The mixture is heated at 42°C and cooled on ice with vigorous vortexing in-between until it becomes clear.

Solution NMR experiments were performed on either a Bruker 600MHz spectrometer or a Varian 800MHz spectrometer, both equipped with a triple-resonance cryo-probe. Solid-state NMR experiments were performed on a Bruker 700MHz spectrometer with a homebuilt double-resonance probe that has either a solenoid coil with strip-shield (Wu 2009) or MAGC coil (Grant 2009). 2D SLF spectra were acquired by using "sammy" pulse sequence (Nevzorov 2003). Data were process using NMRPipe and NMRDraw (Delaglio 1995), and displayed by either NMRView (Johnson 1994). Structure calculation was done by Xplor-NIH (Schwieters 2002).

2.3 Characterization of Vpu by Solution-State NMR

The importance of detergent/lipid optimization for the solubilization of proteins in solution experiments cannot be overstated. It is fortunate that previous works on Vpu described in the introduction have established DHPC as the best agent for all of the constructs. The judgment is based on overall solubility, stability, and

resolution, and the last criterion is by far the most important in terms of spectroscopy. DHPC is a phospholipid that contains a six-carbon acyl chain and a saturated amine head group connected by a phosphate group. It is classified as a zwitterion lipid since the head group and the phosphate are oppositely charged and is thus a mild solubilizing agent comparing to the harsher ones such as SDS. Several existing constructs of Vpu have been re-expressed and re-purified with added optimization procedures to maximize yield and purity. One example of such optimization is an added step of Ni affinity column after the CNBr cleavage of Vpu-cyto to remove the fusion partner and un-cleaved protein. Since the 6X histine tag is on the fusion partner and not cleaved off by CNBr, this step was able to be incorporated to significantly improve the purity of Vpu-cyto. The Figure 2.1 shows the HSQC spectra of full length (A), cytoplasmic (B) and transmembrane (C) constructs of Vpu in 100mM DHPC micelle at pH4 and 50°. The figure shows that all of the spectra are well resolved, and

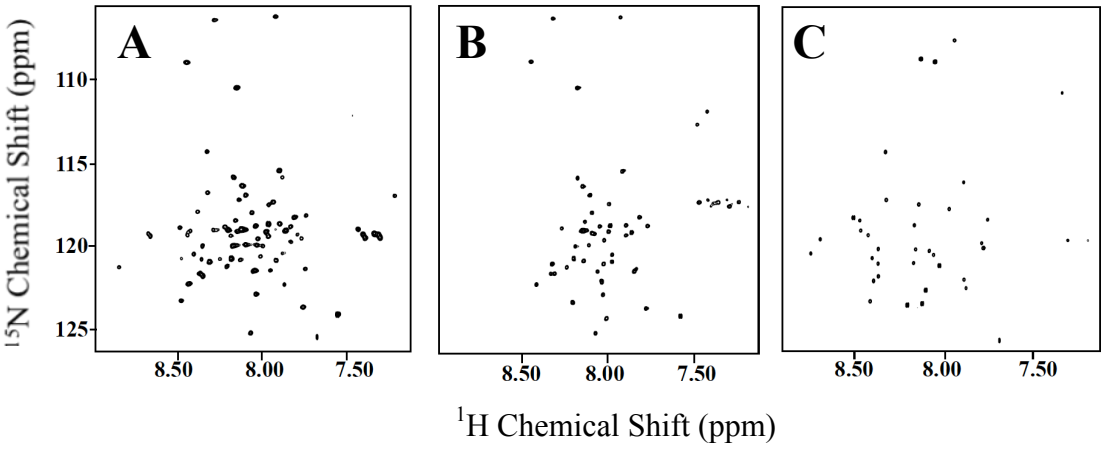

Figure 2.1: Comparison of HSQC spectra of different constructs of Vpu. A, B, and C are Vpu full length, cytoplasmic and TM, respectively. Spectra are acquired in 100mM DHPC micelle at pH4 and 50°C on a Bruker 600MHz spectrometer with a cryo-probe.

this is especially the case for Vpu-TM. The overlap between Vpu-full and -cyto is quite well except for the terminal regions, and the same can be stated for the comparison between full and TM constructs. This suggests that the core structures of the TM and cyto domains are not significantly disturbed when separated from each other. The resonance assignment for all three constructs has been done previously (unpublished), but it is repeated for Vpu-cyto for confirming the assignment and resolving several discrepancy such as unassigned and significantly shifted peaks present in the newly purified Vpu-cyto construct. The backbone amid assignment was performed using triple-resonance HNCA (Grzesiek 1992) and CBCA(CO)NH (Muhandiram 1994) pulse sequences, and confirmed by isoleucine and valine selectively labeled proteins. The strip plots that illustrate the backbone resonances correlation obtained from various slices of the 3D HNCA experiment are shown in Fig2.2 for residues 29-81 of Vpu-cyto. Each strip plot is essentially a 2D spectrum of $^{1}H - ^{13}C\alpha$ correlation from the backbone, and the stronger peak of the pair comes from the intra-residue (residue i) signal whereas the weaker one comes from Cα correlation of the previous residue (i-1). Analysis of the spectra yields the residual assignment of backbone amide proton and nitrogen and Cα atoms. This is the generally the first and required step into any structural and/or functional analysis of the protein, and it is often the most time consuming step as the protein size gets larger.

The secondary structure regions of vpu-cyto can be indirectly mapped by comparing its Cα chemical shifts with that of a random coil, and the analysis is called

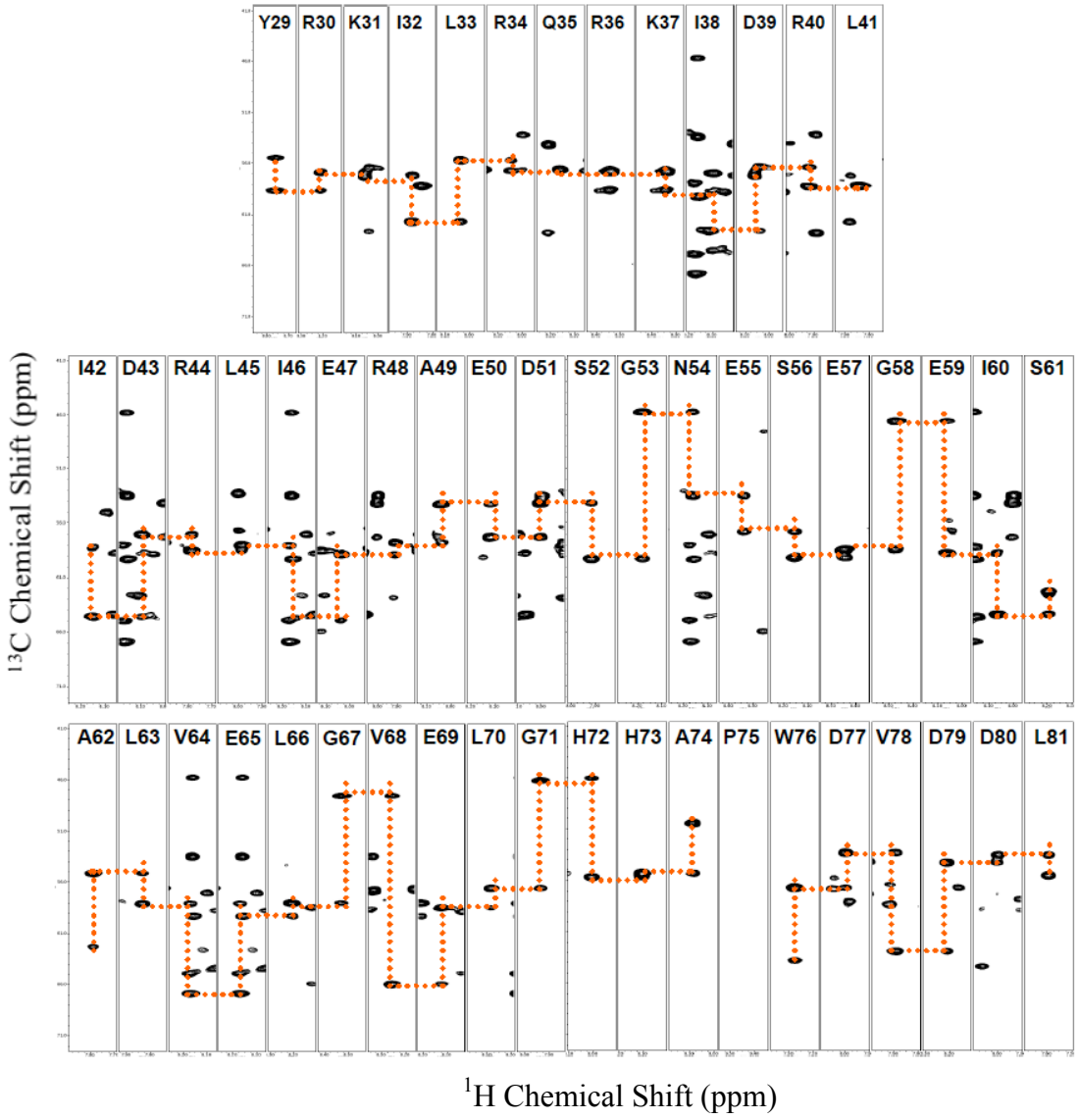

Figure 2.2: Strip-plots from HNCA experiment for Vpu-cyto. Each strip contains a peak from the Cα-HN correlation of the same residue (i) and a peak from Cα of the previous residue (i-1) and the HN from the i residue. The two peaks are connected by the dotted line. The connection between the Cα values of the i and i-1 residues are also shown as the dotted line. This method allows for the resonance assignment of the backbone amide and Cα nuclei.

chemical shift index (CSI) (Wishart 1994). The result is shown in Fig 2.3B with CSI values plotted against the residue number. Positive value shows a tendency of the residue to be in a helix, and negative value corresponds to β-sheet, so consecutive positive values are indicative of a helical secondary structure. While CSI is a relative easy and efficient method to map secondary regions, it is a statistical and thus indirect method. For direct identification of the α-helical regions, we measure the RDC values of the backbone amides. As described in the introduction chapter, RDC gives the angular constraint on the amide bond since the value is orientation dependent. Fig 2.3A shows the RDC values plotted against residue number for Vpu-cyto using stretched polyacrylamide gel. Two dipolar waves can be fitted on the plot, and the helical regions match well with results from the CSI. These two plots are stacked together with the HSQC intensity plot (Fig 2.3C) which is also a indicator secondary structure since peaks in structured regions have lower dynamics than the ones in loop/coil regions and thus have lower intensity due to line broadening. From the overlap shown in blue rectangles in Fig2.3, the helical regions of Vpu-cyto construct spans from residue 37 to 49 and from 58 to 71. This is in contrast with the RDC data for vpu-full construct (unpublished) where the first amphipathi helix spans residue 32 to 49. The shortening of the first helix is likely resulting from the truncation which enables the N-terminal region of the helix to become more mobile and thus disrupts the secondary structure. It is also possible that TM domain has certain stabilizing effects on the first cyto helix. However, it is reasonable to conclude the major structural features are the same for the two constructs which includes two amphipathic

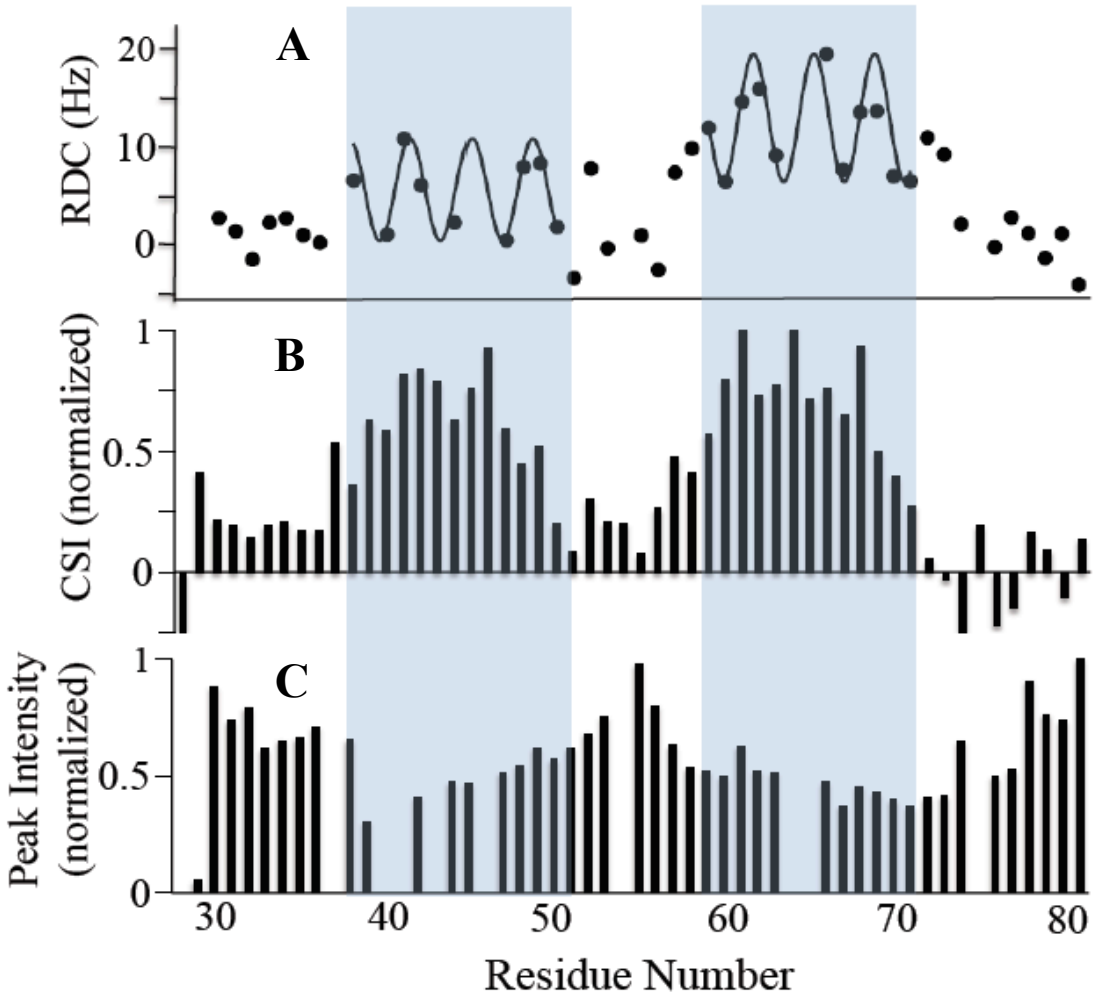

Figure 2.3: Stacking of the RDC, CSI and intensity plots for Vpu cytoplasmic domain. A) RDC values are plotted against residue numbers with dipolar waves fitted. B) Nomalized values for Cα CSI with the positive values indicating a tendency to be within an alpha helical and negative values showing a tendency to be within a beta sheet structure. Consecutive high positive values likely correspond to a helix region. C) The HSQC peak intensities are plotted with the corresponding residues. Lower intensities suggest the residues are within a structured regions where high intensities often correspond to flexible regions such as termini or loop.

helices connected by a very mobile loop which contains two serines necessary for the recruitment of E3 ubiquitin ligase complex.

The dynamics of the vpu cytoplasmic is effectively characterized through the 'q-titration' experiment in which the protein is solubilized by bicelles of increasing size. The 'q' value is the molar ratio of long chain lipids (DMPC) to short chain lipids(DHPC) with q = 0 being micelles, $0<q<1.5$ being isotropic bicelle, and $q>1.5$ being aligned bicelle. As 'q' value increases, the tumbling rate of the lipid aggregate decreases, and that will reflect though the decrease signal intensities of any proteins associating with the lipids. The dynamics of the protein's localized motions and lipid interaction sites will then be reflected through the differential rate of decrease in the signal intensity of individual residues. When interpreting the data, the assumption is that the signal intensity decrease is mainly the result of increased transverse relaxation (T_2) rate which is inversely related to tumbling rate. After uniformly ^{15}N labeled Vpu-cyto was solubilized in lipids of various q values, the backbone signals were monitored with ^{15}N-^{1}H HSQC experiment. The results are shown in Fig 2.4 as an overlay of the spectra under difference q values. A couple of residues are highlighted in separate windows. The plot inside the box on the left bottom of the spectrum shows the overlay of resonance intensities plotted against residues with each set of intensities normalized to the highest intensity within the set. The signals corresponding to the two amphipathic helices decrease more rapidly than the signals from the terminal regions and connecting loop. In fact, their signals completely disappear when q reaches 1 while the flexible regions signals attenuate but remain visible. However, when the q

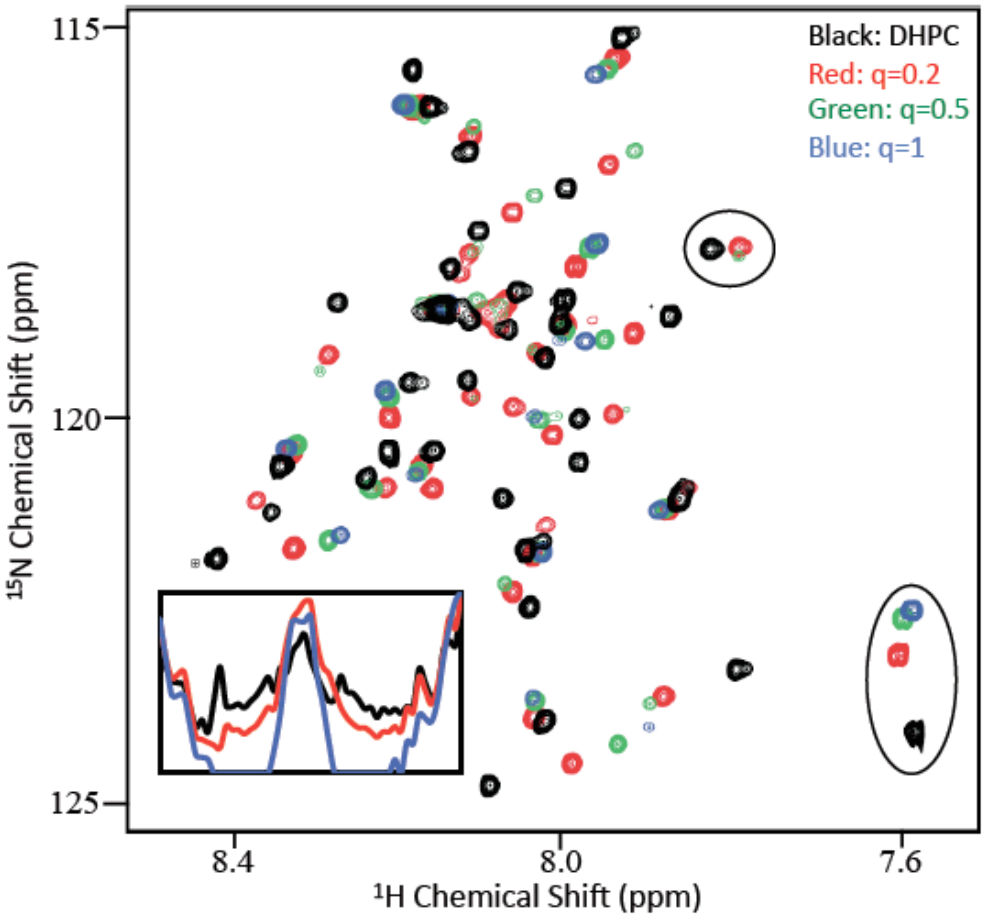

Figure 2.4: 'q-titration' of Vpu cytoplasmic domain. The spectrum is an overlay of four HSQC spectra under different lipid conditions. q is the molar ratio of DMPC to DHPC with 0 being the DHPC-only micelle. q is increased by adding DMPC into the DHPC micelle and resulting complex is a bicelle which tumble more slowly and thus have decreased rotational correlation time. Two sets of the peak changes induced by the q-titration are highlighted by ellipses. The bottom right one is a terminus residue which have significant internal motion so the peak intensity remain relatively strong even when the q value reaches 1 (blue). The other set correspond to a residue within a helical region that binds to the membrane surface, and the peak intensity reduces dramatically when q is 0.5 (green) and is beyond detection when q reaches 1 (blue). The inset box shows the normalized intensity changes under different q conditions. The intensities of the two amphathic helical regions fall off much more rapidly than the terminal and connecting loop. The q-titration method is a fast and efficient way for mapping the secondary structure regions of the proteins that bind to lipids.

reaches 3.2 in which the bicelle becomes magnetically aligned with respect to the magnetic field, none of the backbone signals remain because they are broadened beyond detection. Using solid-state NMR in which q=3.2 is a standard condition for bicelle preparation, the signals can be regained. In addition to the structure characterization, this is a good illustration of the difference in solution and solid-state NMR where the two techniques are developed to study samples under different motion states and can and should be used to complement each other in the characterization.

Since the solution NMR has the ability to monitor signals from individual residues due its high resolution, it is a valuable tool to studying binding interactions by monitoring the chemical shift perturbations resulting from binding of ligand (small molecule, peptide or DNA). Vpu has ion channel activities, so it serves as a good target for channel blockers as potential anti-viral drugs. Amiloride and its derivatives were previously shown to block ion transport activity of Vpu (Ewart 2002). HSQC spectra were recorded for Vpu-TM in DHPC micelles with 0, 10, and 40mM 5-(N,N-dimethyl) amiloride (DMA), and the overlay of the expanded region of the spectra is shown in Fig2.5A. It shows evidence for residue specific interaction between protein and drug molecule as certain peaks experience significant perturbation whereas others undergo almost no changes. The calculated chemical shift difference between 0 and 40mM DMA are plotted against residues and shown in Fig2.5B. Residues 22-27 on the C-terminal region appear to be affected most by the presence of DMA and thus may serve as an important binding site. The rest of the Vpu-TM experiences minimal perturbation except for residues 4, 10, and 20 which have relatively moderate

chemical shift changes. These results demonstrate a common and efficient technique for screening drug binding and identifying the binding sites.

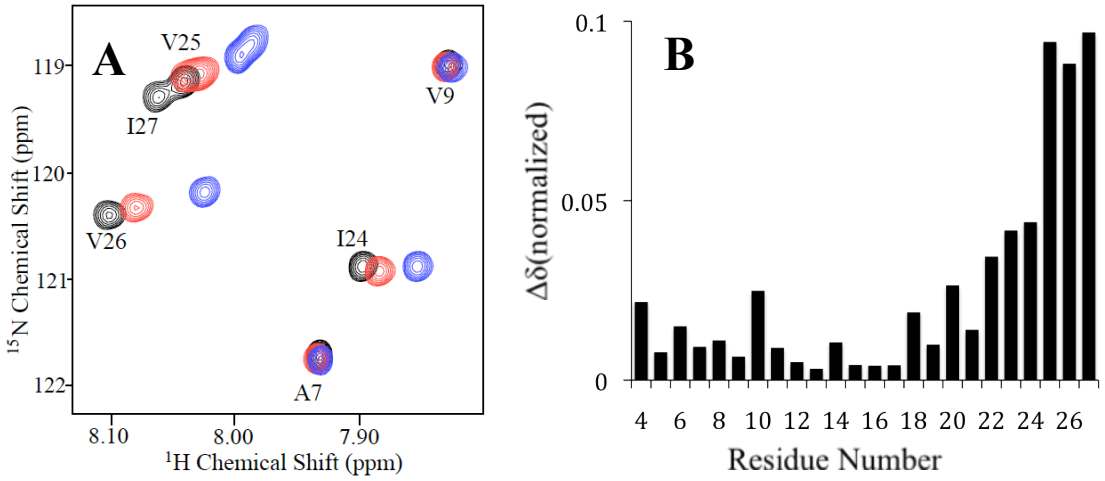

Figure 2.5: Drug interaction study between Vpu-TM and DMA, a channel blocker for Vpu. A). Overlay of the partial HSQC spectra of Vpu-TM with 0, 10, and 40mM DMA colored as black, red, and blue, respectively. The movement of the peaks shows specific residue interaction with the drug molecule. B). Chemical shift perturbation (Δδ) values are plotted against the corresponding residue numbers showing the C-terminal residues are most affected by the drug binding.

2.4 Summary and discussion

'Divide and conquer' is a frequently used strategy in the structure determination structure of macromolecules whereby a large molecule is made into smaller components through truncation. Even though Vpu is a relatively small protein of around 80 amino acids, previous experiences have shown that 'divide and conquer' is necessary and effective for characterizing this protein not only because it is a membrane protein but also because it has very unique and challenging structural and dynamic features. Its cytoplasmic domain has high degree of flexibility whereas the TM domain is a relatively rigid helix but also can form oligomers. Solution NMR has been proven very successful in identifying the secondary structure regions of various

constructs of Vpu through the use of RDC, chemical shifts, and ‘q-titration’. However, for determining the three dimensional structure, it is a challenging task for the cytoplasmic and full length constructs likely due to the added dynamics. More constraints, especially long-distance ones, are needed, and one of the methods to obtain the constraints is PRE which involves covalently attaching paramagnetic label to a cysteine residue and then observing the line broadening effect as a function of the proximity to the paramagnetic center. There are already promising results for using this method to generate a preliminary structure of the Vpu cytoplasmic domain in micelle, and efforts are also being applied to the full length construct.

For characterizing Vpu in bicelles, solid-state NMR has been instrumental in advancing the structural knowledge as it produced the first structure of Vpu TM domain within a bilayer environment (Park, 2003). The spectral resolution and sample stability from the TM studies are also unmatched in comparison to other magnetically aligned bicelle proteins except for a few cases. Unfortunately, the same level of success has not yet been translated onto the Vpu full length and cytoplasmic constructs as both samples lack the adequate resolutions to provide useful structure information. Considerable amount of efforts have been spent on improving the sample and spectral quality with no significant improvement from previous results, so they are not described in this thesis. However, one can still draw certain conclusions from the efforts. One is that the cytoplasmic domain not only has considerable amount of dynamics by itself but also adds significant motion/dynamics to the transmembrane region as part of the full-length. In addition, this motion is in the NMR acquisition

time scale (~0.5-5ms) because it contributes significantly to the spectral quality. It is not known whether the full-length construct exists as a oligomer in bicelle and whether this oligomerization can have motions that affect the spectrum. It, however, can be concluded from the 1D chemical shift anisotropy that the TM of the full length is at least inserted into the bilayer in comparison to the surface binding cytoplasmic construct. There are still strategies one can try to resolve the resolution and dynamics issue. One is to stabilize the Vpu cytoplasmic domain through lipid composition optimization and/or a binding partner such as a protein or ligand. The other is to increase the dimension of the experiment to 3D or even 4D to resolve the crowded regions on the 2D spectrum. Both of these two efforts are on going by other members of Opella group, with the higher dimension experiments showing especially promising results.

Chapter 3. Comparison of Two Viroporins, Vpu and M2

3.1 Introduction

There is a group of proteins that can be classified as viroporins. As the name suggests, these proteins have two important characteristics: 1) they are encoded by a viral genome and 2) they exhibit ion channel activities. Viroporins are small (60-120 aa) viral membrane proteins, but they perform crucial functions in the life cycle of the virus. The wildtype proteins are often in the form of homo-oligomers in order to perform the ion channel function. Some examples include HIV-1 Vpu, HCV p7, Influenza A/B M2, Picornavirus 2B, and Alpha Virus 6K (Wang 2011). As described in Chapter 2, Vpu is expressed by HIV-1 and certain SIV related viruses to perform the function of CD4 down-regulation and facilitation of virus release. While it exhibits ion channel activities when incorporated into an artificial membrane environment, it is still unknown if and why Vpu has this activity in vivo.

Among all of the viroporins, M2 proton channel from Influenza A virus is by far the best characterized one in terms of both structure and function. Similar to Vpu, The protein has around 100 amino acids and consists of a small N-terminal domain, a single transmembrane helix, and a cytoplasmic domain. It responds to the pH change in the N-terminal (ectodomain) side by opening the channel when the pH becomes less than 6.5 (Pinto 2006). This is a crucial step in the process of releasing viral genome into the cytoplasm of the host cell as the virus is engulfed in the endosome after entry and endocytosis. The lowering of pH within the endosome triggers the M2 channel to open and allow the influx of protons into the viral interior, and this acidifying process

a prerequisite for the uncoating of the virus. A number of high-resolution structures of the transmembrane (TM) domain have been published (Stouffer 2008, Schnell 2008, Sharma 2010) using a variety of techniques including X-ray crystallography and solution and solid-state NMR. The results consistently showed that M2 is a homo-tetrameric protein with the proton selective gate formed by coordinated conformation of a histidine and a tryptophan within the HXXXW motif. The tryptophan is essential for the gating function of the channel as mutating out the residue abolishes the ability of the protein to regulate the opening and closing of the channel (Tang 2002). The histidine residue is responsible for the protein's high selectivity for protons, and mutation at the histidine site causes the channel to be non-specific allowing other ions such as K^+ and Na^+ to flow through. Interestingly, one study has shown that the selectivity of the histidine substitution mutant can be partially rescued by introducing high concentration of imidazole buffer (Venkataraman 2005). Presumably, the imidazole molecule was able to act in place of the missing histidine side chain which is responsible for the selectively binding and transferring of proton.

The underlying mechanism of the biological functions of Vpu, a structural analogue of M2, is poorly understood. Moreover, there is no high resolution structure for the wildtype full length protein or the oligomeric form of the transmembrane domain. However, one can gain very valuable insights into the structure and function through the strategy of parallel comparison between Vpu and M2. Using M2 as a well studied reference, the similarities and differences can be applied to Vpu to reveal the structure and function through comparative studies. While it is valuable to compare

the results from literature on these two viroporins, it is important and even imperative to have the comparative studies done under same experimental condition to avoid introducing unwanted discrepancy. One of the most important conditions for membrane proteins is the lipid environment, but experiments from various literature sources were often done under different lipid conditions rendering the parallel comparison between them to be error-prone and not straight forward. As the protein-lipid interaction is still not well understood, it is important to eliminate the discrepancies in experimental conditions as much as possible.

Two previous studies have demonstrated the possibility of converting Vpu-TM to mimic the M2-TM through a single mutation (Hout 2006, Park 2007). The motivation behind the studies is based on the similarity in the amino acid sequence of the two TM domains. They both have the hydrophobic residues and have the perfectly conserved tryptophan residue towards the C-terminus. Fig 3.1 below shows the sequence alignment

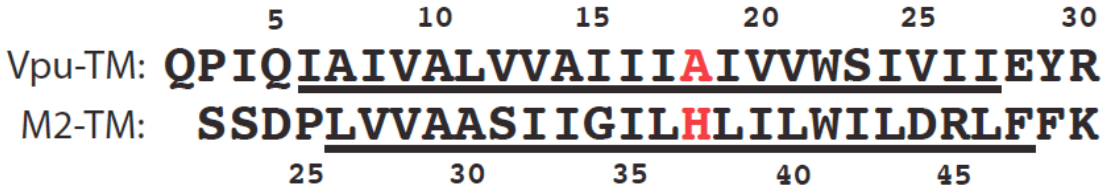

Figure 3.1: Amino acid sequence alignment of Vpu and M2 TM regions. The transmembrane helical regions are underlined. The main difference between the two is the residue three positions away from the conserved tryptophan residue as indicated with red color.

of the two with the TM helical region underlined. The noticeable difference, colored in red, between the two is the residue positioned three residues away from the tryptophan. M2 has a histidine whereas Vpu has an alanine at that position. Work done

by Hout and coworkers (Hout 2006) showed that mutating the alanine to histidine mutation makes Vpu susceptible to rimantadine which inhibits the channel activity of M2 but previously had no effect on Vpu. More specifically, the ability for mutant Vpu to facilitate the release of mature virions was significantly impaired in the presence of rimantadine. NMR studies by Park and coworkers (Park 2007) in micelles and bicelles showed that the Vpu A18H mutant displayed susceptibility to rimantadine binding from the chemical shift perturbation results. More interestingly, the mutant have a helix tilt angle of 41°, 11° larger than that of the wildtype in bilayer. This large change in tilt is quite remarkable considering the restrictive nature of the membrane.

In order to investigate whether this phenomenon is reversible on M2, two constructs of the TM domain of A/M2 are made. One contains the wildtype sequence that includes residues 22 to 49 with five extra lysines attached to the C-terminus solubilization tag, and the other has the His37 residue mutated to alanine to mimic wildtype Vpu-TM. The proteins are subjected to the same solution and solid-state NMR experiment to characterize their difference in structure, drug binding, and topology. In addition, the sensitivity to proton concentration is also examined by solution NMR.

3.2 Material and Methods.

Unless stated otherwise, the protein expression and purification has been described previously in Chapter 2, and NMR sample preparation and experiments also follow the procedure described in that chapter. Mn-EDTA solution was prepared by

first combining $MnSO_4$ and EDTA solution with EDTA in slight molar excess and then washing the resulting precipitate with methanol and ethanol. Finally, the precipitate was lyophilized and dissolved in 1M HEPES buffer (pH=8) to make a stock solution. The chemical shift difference ($\Delta\delta$) is calculated using the formula shown below with δ_H and δ_N being the proton and nitrogen chemical shift, respectively.

$$\Delta\delta = \sqrt{(\Delta\delta_H)^2 + (\Delta\delta_N/5)^2}$$

3.3 Comparison of Vpu and M2 in Micelles by Solution-State NMR

HSQC spectra of ^{15}N uniformly labeled wt M2-TM and H37A mutant in 100mM DHPC at pH4 are shown in Fig 3.2. As in the case of Vpu-TM constructs, they yield well resolved backbone amide resonances that allows for the monitoring of individual residues. All of the backbone signals are assigned with 3D experiments described in Material and Methods, and further confirmed by selectively labeled amino acids sample. Several properties of the protein-micelle complex are investigated including pH effect and drug binding. In each case, experimental results of M2 constructs are compared with either previously published results or newly acquired data of Vpu constructs.

Since M2 is a proton channel, its sensitivity to proton concentration has been well documented. Using solution NMR, this property can be probed by the chemical shift perturbation as the result of pH change of the aqueous environment. This is

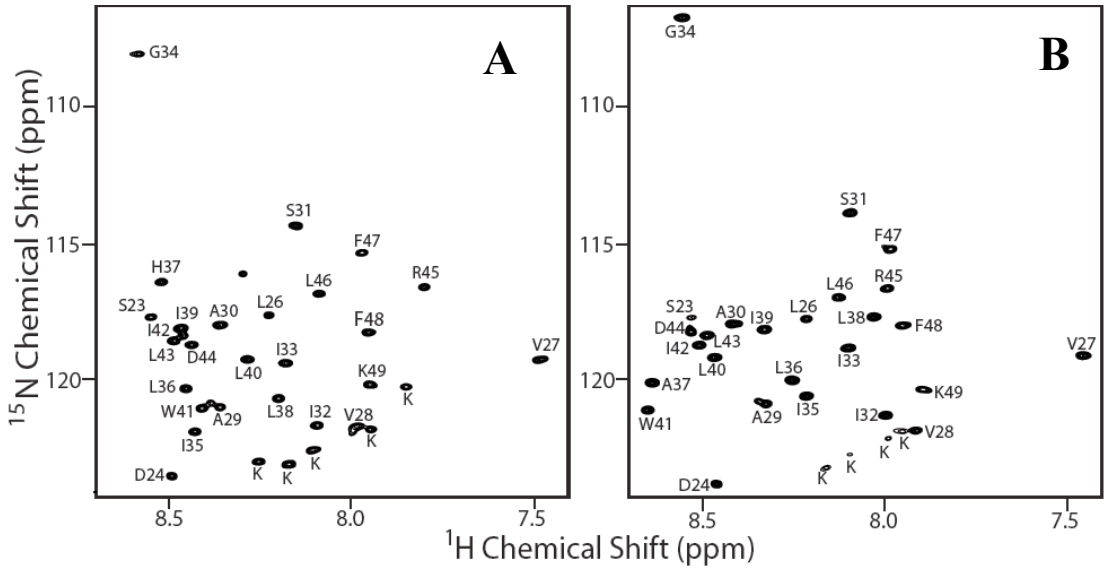

Figure 3.2: HSQC spectra of wt M2-TM(A) and M2-TM H37A mutant (B). The proteins are in 100mM DHPC micelle at pH4 and 50°C. 2048 and 256 points are acquired in the proton and nitrogen dimensions, respectively. The full resonance assignments are indicated by the peak labels and done with triple-resonance HNCA and HN(CO)CA experiments. The C-terminal lysine peaks are not assigned as they are not part of the native sequence.

demonstrated by the plot of change in chemical shift (Δδ) against the residue number shown in Figure 3.3A for wildtype M2-TM when pH is changed from 4 to 7.5. Large

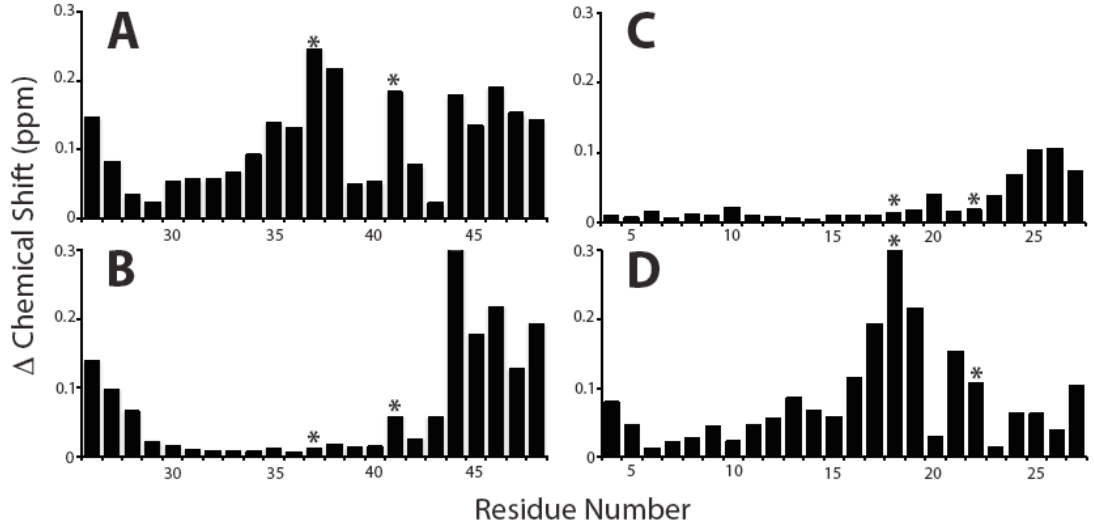

Figure 3.3: HSQC chemical shift perturbation plots of Vpu-TM and M2-TM constructs induced by change in pH from 4 to 7.5. The positions of the alanine, histidine and tryptophan residues within the (H/A)XXXW motif are indicated by the asterisk. The constructs are wt M2-TM (A), M2-TM H37A mutant (B), wt Vpu-TM (C), and Vpu-TM A18H mutant (D). Constructs that contain the HXXXW motif (wt M2TM and Vpu-TM A18H) show significant chemical shift perturbation for that region while the constructs that contain the AXXXW motif show no response for the same region as the result of pH change. Results confirm the role of histidine as the proton filter in an ion channel.

chemical shift change associated H37 and adjacent residues are consistent with other findings that point to the histidine residue as the proton filter. The large change associated W41 residue confirms the importance of the HXXXW motif as a cooperative mechanism for proton transport. An interesting observation is the relative large change with residues 44-48 which are not directly implicated in the proton channel activity. Their sensitivity to proton concentration suggests that they may also play a role in the proton transport. In comparison, the H37A mutation yielded a

dramatic difference in terms of the proton sensitivity as shown in Fig3.3B where both A37 and W41 have minimum chemical shift perturbation in response to the pH change. This is a clear indication that the residues have lost the sensitivity to proton and consistent with previous findings that mutations introduced on the histidine residue causes M2 to lose the selectivity for proton and permit the flow of other ions such as K^+ and Na^+ (Venkataraman 2005). However, residues 44-48 still have relative large chemical shift change. It is unclear weather they are involved in the proton transport, but one can at lease conclude that the loss of proton sensitivity due to H37A mutation is not conferred on these residues.

In the case of Vpu, the wildtype TM is not expected to have the sensitivity to proton concentration change, and the results are in agreement with the expectation (Fig 3.3C). There are minimum chemical shift differences except for the few residues at the C-terminus, and the magnitude of change associated with those residues is relatively small comparing to M2. A18H mutant contains the HXXXW motif, so it is expected to be proton sensitive, and the result shown in Fig 3.3D confirms that. Like wildtype M2, the histidine residue has the greatest change in the chemical shift value while the adjacent residues also has large chemical shift difference in response to the pH change. The tryptophan (W22) residue in the A18H mutant has moderate change in the chemical shift, but not as dramatic as in the case of wildtype M2. This suggests that the residue may not be as cooperative with the histidine as the tryptophan (W41) in M2, and the protein may be less efficient in its proton transport activity. The important conclusion drawn from the comparison is that the proton sensitivity can be

conferred to Vpu by mutating the alanine residue to artificially generate the HXXXW motif. The chemical shift difference pattern of the mutant becomes very similar to the wildtype M2 but with some differences, especially regarding the tryptophan residue.

Rimantadine is an admantane derived drug used for treating infections caused by Influenza A virus though it is no longer recommended for use today because high level of resistance that the virus has acquired over time. However, it is still very valuable to study its mechanism of action in order to develop more effective anti-viral drugs. Rimantadine works by targeting the ion channel formed by M2 presumably to block its proton channel activity and prevent the RNA release process. Previous NMR study has shown that the rimantadine caused significant chemical shift perturbation for the Vpu-TM A18H mutant, notably residues 15 and 18 while it had minimal effect on the wildtype TM in DHPC micelle. In the case of M2 constructs shown in Fig 3.4, there is no significant difference in the perturbation profile between the wildtype (A)

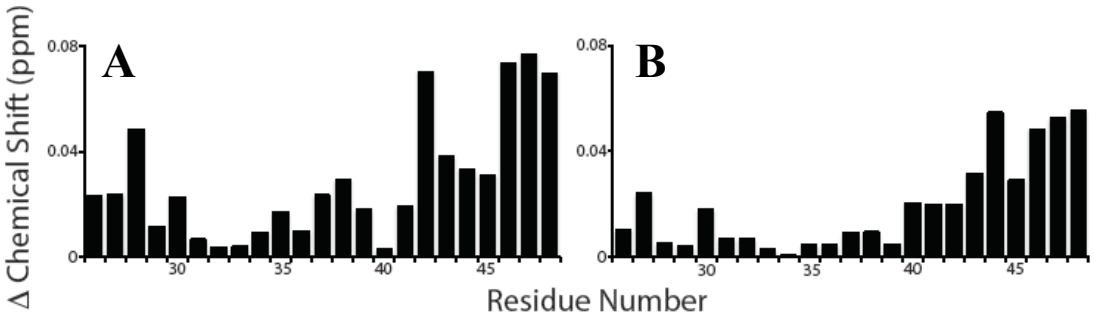

Figure 3.4: HSQC chemical shift perturbation plots of M2 constructs in response to rimantadine binding. Chemical shift differences are calculated for wt M2-TM (A) and M2-TM H37A mutant (B) with and without the presence of 40mM rimantadine in DHPC micelle. The C-terminal regions for both constructs show significant perturbation. The HXXXW motif region showed relatively moderate response for wt M2TM while the corresponding region for H37A mutant experience minimum perturbation.

and H37A mutant (B) though there are moderate differences localized between residues 36-38. This suggests that the binding site(s) are similar between the two constructs, but the chemical environment around the histidine residue in the wildtype TM is a little more perturbed by rimantadine. Past studies on the exact binding site of rimantadine/amantadine on M2 have yielded certain conflicting results. In both X-ray and solid-state NMR studies, the drug molecule is shown to reside in the N-terminal portion of TM and inside the channel pore (Stouffer 2008, Sharma 2010). In a solution NMR study (Schnell 2008), the drug is shown to bind to C-terminal region of the TM and on the outside surface of the channel. In this study, both wildtype and mutant M2 exhibit large chemical shift perturbations for residues on the C-terminal region which is consistent with the solution NMR study mentioned above. One hypothesis is that this region is outside of the micelle and thus more susceptible to perturbation by the agents in the solvent environment. To test this hypothesis, Mn-EDTA is added to the sample to identify the residues exposed outside of the micelle coverage. Mn-EDTA is a paramagnetic metal chelate that broadens the peak of the nucleus that it comes to close contact with through paramagnetic relaxation enhancement. Since the compound is too bulky to enter the micelle, it affects only the residues exposed. The residues most significantly affected by the presence of Mn-EDTA are 27 and residues C-terminal of 43 (data not shown). This confirms the increased exposure level for the C-terminal residues and may offer an explanation for the observed chemical shift perturbation pattern in the presence of rimantadine.

3.4 Comparison of Vpu and M2 in Bicelles by Solid-State NMR

Previous published result showed a significant difference in the tilt angle between wildtype Vpu-TM(30°) and A18H mutant (41°) when incorporated into bicelles. In addition, it was observed that the helical length for the A18H mutant is four residues longer than the wildtype. To compare these results, wildtype M2 and H37A mutant are incorporated into the DMPC/DHPC bicelle prepared identically, and solid-state NMR experiments were acquired under the same condition. Fig3.5 shows the 2D ^{15}N chemical shift/^{1}H-^{15}N dipolar coupling spectra of the M2 constructs (A and B) and the previously recorded spectra for Vpu (C and D) constructs as comparison. In general, all of the spectra have good resolution with the peak linewidth around 2ppm in the ^{15}N chemical shift dimension and 300Hz in the dipolar coupling dimension. Tilt angle of the construct can be determined by fitting Polar Index Slant Angle (PISA) wheels onto the spectrum. As described in Chapter 1, the dimensions and the location of the PISA wheels are dependent on the tilt angle of the helix. In the figure, they are superimposed onto the spectrum as dashed ellipses. Based on the best fitting, the tilt angles are 28°, 38°, 30°, and 41° for wt M2-TM, M2 H37A, wt Vpu-TM, and Vpu A18H, respectively. This confirms that the approximate 10° change caused by the histidine is reversible in M2, and there is 8° difference between the TM domains of wildtype Vpu and M2. The consistency is remarkable in terms of both the change in the tilt from wildtype to mutant and the similarity between the wildtype of one viroporin and the mutant of the other. Result suggests that the tilt angle of A18H mutant of Vpu is similar to that of wildtype M2 and vice versa.

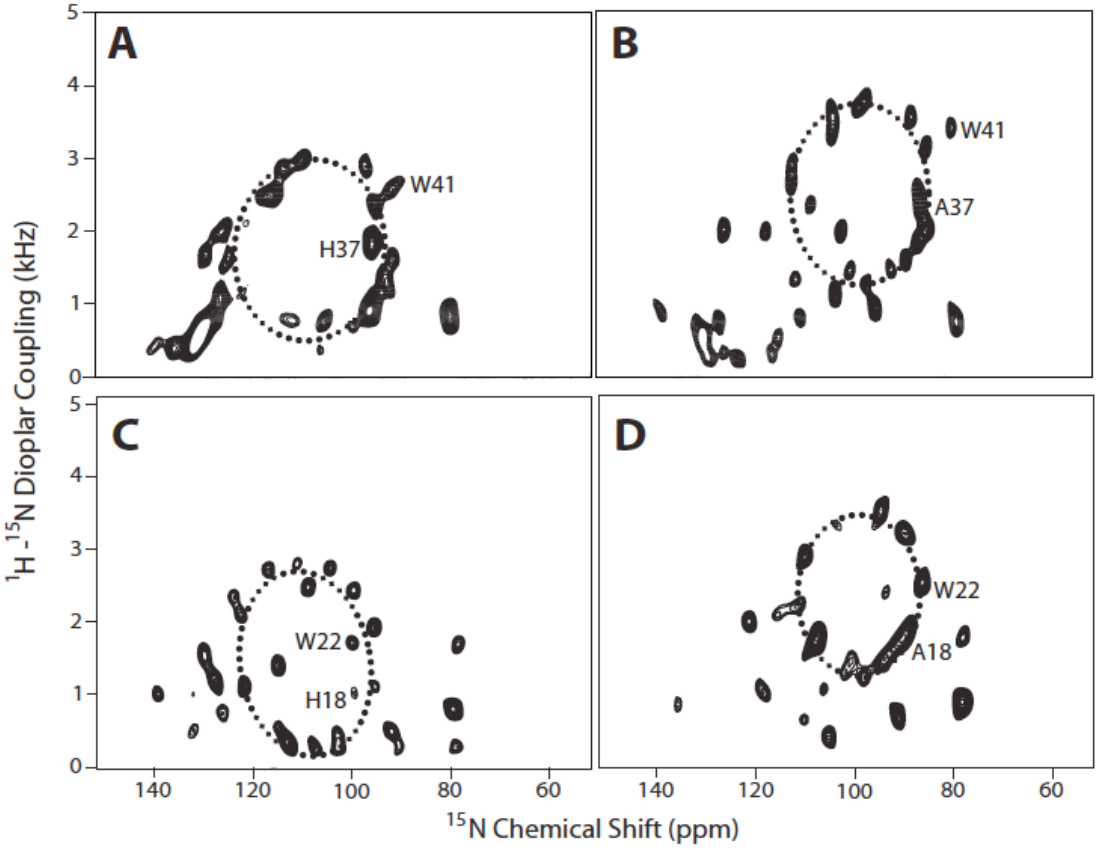

Figure 3.5: Comparison of 2D ^{15}N chemical shift/^{1}H-^{15}N dipolar coupling spectra for ^{15}N uniformly labeled Vpu and M2 constructs. All spectra are acquired on proteins incorporated into DMPC/DHPC bicelle and magnetically aligned in a 700MHz Bruker spectrometer at 40°C. PISA wheels are fitted onto the spectra as dashed ellipses. The helix tilt angle estimated from the wheel fitting are 28°, 38°, 30°, and 41° for wt M2-TM (A), M2 H37A (B), wt Vpu-TM (C), and Vpu A18H (D), respectively (Park 2007).

The full resonance assignment for the Vpu constructs have been done in the previous published work. Assignment for the M2 constructs are achieved through selectively labeled samples shown in Fig3.6. For simplicity of the display, only the positions of the tryptophan and histidine/alanine are indicated on the spectra. This is enough information to compare the rotation angle of the helices, and the comparison shows that the angle is very similar between wildtype and the mutant, and slight difference of about 15° between Vpu and M2. It suggests that the Vpu and M2 may have slightly different packing face in terms of oligomerization but it is still consistent with the notion that tryptophan is important for the gating of ion channel even in the case of Vpu because the location of tryptophan on the helical wheel is not dramatically different between the two viroporins.

2D spectra for the ^{15}N selectively labeled leucine spectra for M2 constructs are shown in Fig3.6, and all of the resonances are resolved. From the relative positions of the resonances, one can find the best fit of the helical rotation angle by comparing the peaks to the helical wheel representation of an ideal helix. While all of the residues show up in the case of the H37A mutant (Fig3.6B), but the L40 residue is missing in the wildtype M2-TM spectrum (Fig3.6A). One possible explanation is that the backbone amide of the residue has added dynamics that broadens the peak due to the chemical exchange and lowers the dipolar transfer efficiency. L40 residue is absolutely conserved across all strains of M2, and it was shown to be important in the tetramer stabilization (Stouffer 2005). To further confirm the relative placement of the residues on the helical wheel, the M2 H37A leucine sample was hydrated with 90%

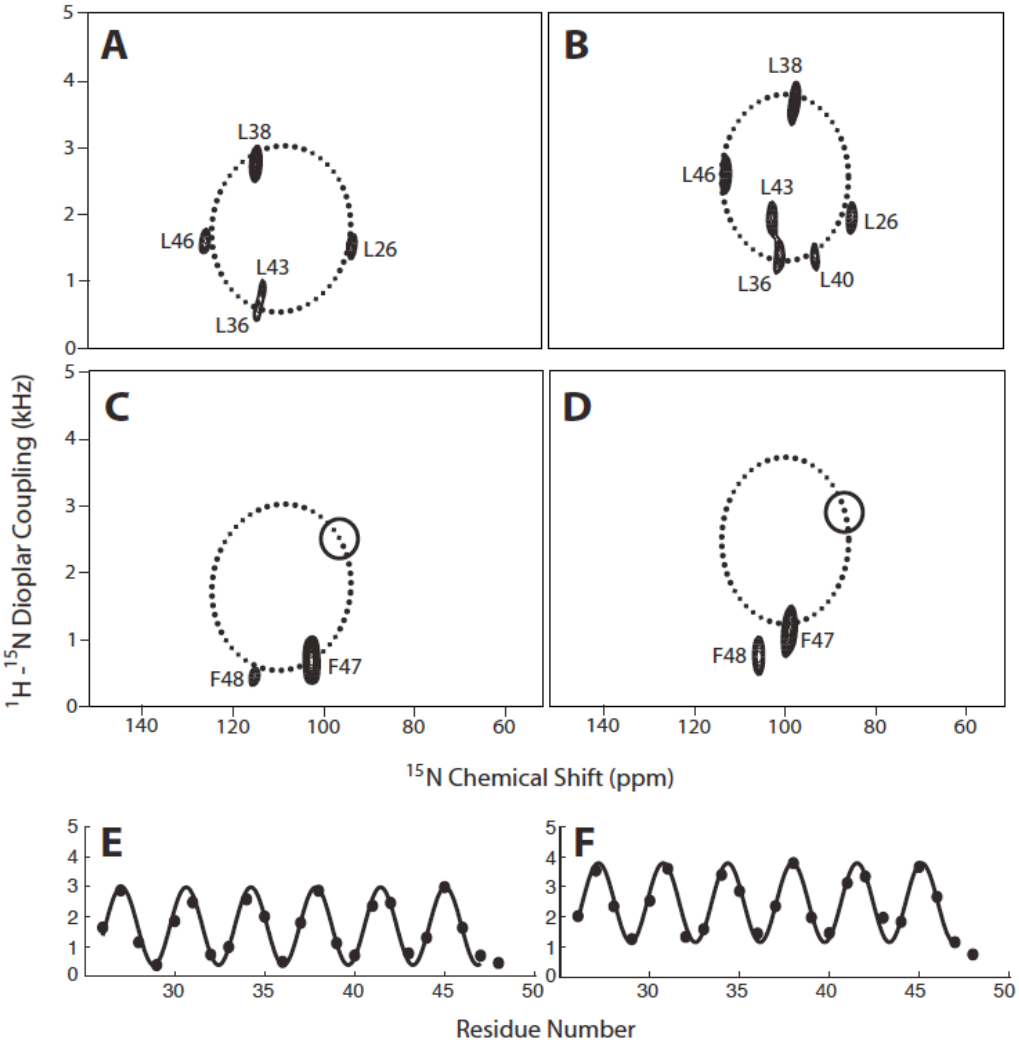

Figure 3.6: Selectively label 2D ^{15}N chemical shift/^{1}H-^{15}N dipolar coupling spectra and dipolar waves for M2-TM constructs. ^{15}N Leu spectrum of wt M2-TM and H37A mutant are shown in A) and B), respectively. ^{15}N Phe spectra of wt M2-TM and H37A mutant are shown in C) and D), respectively. The wheel fittings from the corresponding uniformly labeled samples are superimposed on the spectra as dashed ellipses. Assignments are made by comparing the positions of the peaks to the expected positions on an ideal helical wheel. All of the leucine residues show up in the H37A mutant spectrum shown in B), but L40 is missing from the spectrum in A) for wt M2-TM, perhaps due to dynamics of the residue. Peaks for residue F47 show up at expected position for both constructs where as position for the F48 peak has significant deviation indicating the end point of the TM helix. RDC plot and dipolar wave fittings for wt M2-TM and H37A mutant are shown in E) and F), respectively. Both have close to ideal helical conformation and the same helical length of 22 residues.

D_2O. The disappearance of peaks for L26 and L46 indicate that these two are in the terminal regions of the helix and susceptible to D_2O exchange (data not shown). The PISA wheel fittings from the uniformly labeled spectra are transferred onto the corresponding leucine spectra, and all of the peaks are located close to the traces of the fitting. This is an indication that they are within the same helical region, and the helix spans minimally from L26 to L46. Residue 25 is a proline which is often located at the ends of the transmembrane helix and a known helix breaker, so L26 can be concluded as the start of the helical region. To identify the C-terminal end, ^{15}N labeled phenylalanine samples are prepared since the lysine tag is known to be charged and unstructured and would not contribute to the transmembrane helix. The resulting spectra shown in Fig3.6C and D give clear evident that F47 is the C-terminus residue for both wildtype and mutant. The peak for F47 falls within the expected region on the spectrum and with respect to the PISA wheel, but F48 is located well outside of the expected region on the spectrum which is indicated by the open circle. Therefore, the overall results show that wildtype and H37A mutant have the identical helical span of 22 residues from L26 to F47. Fig3.6 E and F show the dipolar wave fitting of the dipolar coupling values plotted against residue number for the wt M2-TM and H37A mutant, respectively. The residues 26 to 47 can be fitted well with a single wave which confirms that the transmembrane domain is a single 22 residue helix with no significant deviations from an ideal helix.

The determined helical lengths of the M2 constructs are the same as the Vpu A18H mutant, but wildtype Vpu-TM was previously found be only 18 residues. This

discrepancy prompted more detailed investigation on the initial conclusion on the helical length of wildtype Vpu-TM. In the previous study, selectively labeled isoleucine spectra were used to determine the length since isoleucines residues are present throughout the TM region. Based on the resonance assignment made in the study, it was concluded that ILE4, 26, and 27 were missing from the spectrum and thus not within the helical region of the wildtype Vpu-TM. In comparison, all isoleucine residues were present and fall within the PISA wheel region in the A18H mutant spectrum. Upon further analysis of the isoleucine spectrum for wildtype TM, an alternative assignment could be made so that 'missing' residues can be designated within the spectrum. The ambiguous assignment situation mainly arises because of inadequate resolution of the peaks. To confirm that there is indeed a mistake in the original assignment, another mutant of Vpu was constructed to replace I4 with L4

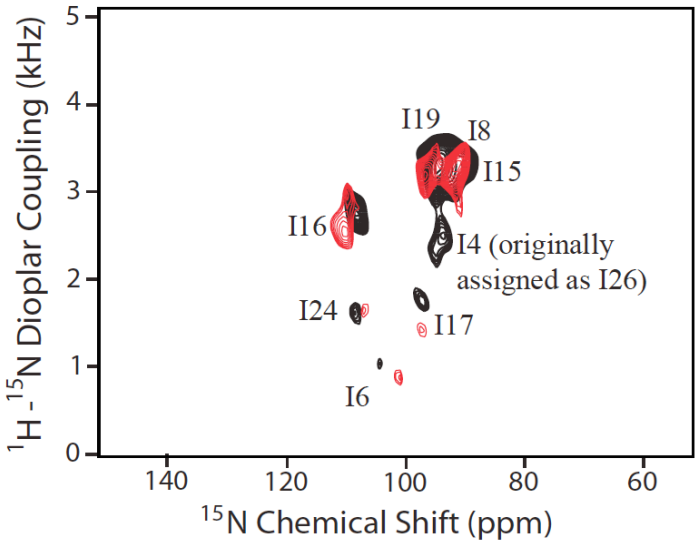

Figure 3.7: Overlay of 2D ^{15}N chemical shift/H-N dipolar coupling spectra of ^{15}N Isoleucine wt Vpu-TM (black) and Vpu-TM I4L mutant (red). The missing peak in the red spectrum in comparison to the black spectrum indicates the position of the I4 residue.

because peak originally assigned as I26 is actually I4 according to the new assignment. Therefore, the isoleucine spectrum of I4L mutant would have the residue I4 missing so that its position can then be confirmed. Fig3.7 shows the superimposed isoleucine spectra of wildtype Vpu (black) and Vpu I4L mutant. Result indicates that the peak corresponding to residue 4 was indeed miss-assigned in the original data. Further mutational and spectroscopic experiment would be needed to unequivocally confirm that the helical length of the wildtype and A18H mutant Vpu are the same, but the results at least give direct evidence that length of the wildtype Vpu-TM was underestimated. This supports the notion that histidine is, in large part, the only factor responsible for the difference in the tilt angle between the wildtype TM and the corresponding mutant.

A curiosity question that one may raise is whether tryptophan plays any role in the tilt angle. In other words, is the HXXXW motif required in addition to histidine to maintain such high tilt angle within the bilayer? To address this question, a mutant of M2-TM was constructed to replace the tryptophan41 residue of the wildtype TM with a leucine. Since leucine also has a relative bulky hydrophobic side chain, it would introduce minimal perturbation to the structure of the helix. ^{15}N uniformly labeled W41L mutant was incorporated into the bicelle and result of 1D ^{15}N chemical shift spectrum (B) is compared with the that of the wildtype TM (A) as shown in Fig3.8. The well-matched spanning region (indicated by the dashed lines) of the chemical shift anisotropy is a clear indication that the tilt angle for both constructs are the same.

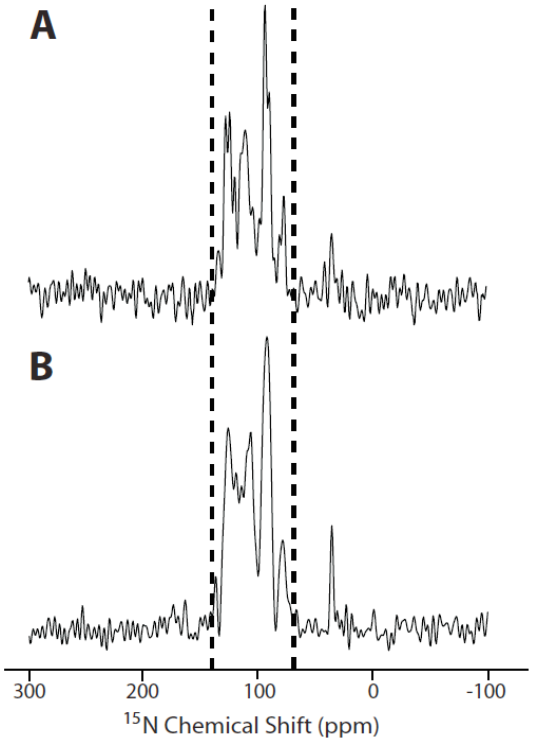

Figure 3.8: Comparison of 1D ^{15}N chemical shift spectra of wt M2-TM (A) and M2TM W41L mutant (B). The dotted line show that the signals for both constructs pan approximately the same region of chemical shift thus indicating the two have similar helix tilt angle.

Unfortunately, the 2D experiment did not yield adequate resolution to allow for the fitting of PISA wheel as most of the signals are aggregated around the low dipolar coupling area. This suggests that the mutant has added dynamics that disrupted the efficient magnetization transfer through dipolar coupling. Tryptophan is known for having the lipid surface anchoring function for transmembrane helix (Planque 2003). The result shows that only histidine is necessary for maintaining large helix tilt angle, but removing the tryptophan causes perturbation on the stability of the protein within the bilayer.

3.5 Conclusion

Comparative studies of Vpu and M2 using solution and solid-state NMR revealed important similarities and differences between these two viroporins. While these two proteins come from different types of virus and have different biological functions and ion channel activities, the differences can be largely traced to a single amino acid. Namely, the residue three positions away from the conserved tryptophan in the N-terminal direction, and the residue is alanine and histidine for Vpu and M2, respectively. This seemingly minor difference results in large change in the proton sensitivity of the TM domain, rimantadine binding susceptibility, and helical tilt angle. The findings in the current work can be summarized through two models of ion channel shown as cartoon in Fig3.9. One model is a proton channel that contains the HXXXW motif towards the C-terminal part of the transmembrane as in the case of wildtype M2 and Vpu A18H mutant. It selectively opens gate in response to low pH and allows the flow of only protons, and it has a tilt angle of approximately 40°. The other model is a non-specific channel that allows the flow of monovalent cations such as Na^+, K^+ as well as H^+, and it contains an AXXXW motif. The helix tilt for this channel is approximately 30°. This strategy of comparative study can be applied to other proteins as well. As demonstrated, this approach is very helpful if one of the proteins has been extensively studied, and the two share very similar features such as topology or secondary structural regions. It is also important to re-emphasize that the experimental conditions should be consistent when comparing the results in order to avoid complications.

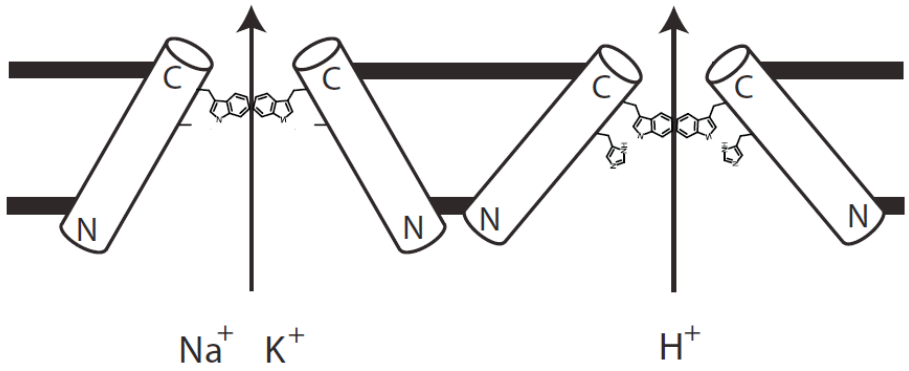

Figure 3.9: Models of two types of ion channels. Left one contains an AXXXW motif in the sequence and is a non-specific cation channel as in the case of wt Vpu-TM and M2-TM H37A mutant. The right one contains a HXXXW motif and allows proton only flow as in the case of M2-TM and Vpu-TM A18H mutant.

Chapter 3, in part, is currently being prepared for submission for publication of the material. Wang, Y., Park, S.H., and Opella, S.J. The dissertation author was the primary investigator and author of this material.

Chapter 4. Elucidation of Protein-Protein Interaction between Transmembrane Domains of Vpu and BST-2

4.1 Introduction

BST-2/Tetherin/CD317 is an interferon alpha induced human restriction factor whose primary function is to prevent the release mature virus particle from leaving the host cell membrane (Van Damme 2008). Its ability to tether the virus to the cell membrane and to each other yields the nickname of 'tetherin', and because of that ability, it serves as an attractive target for anti-viral drug development. The exact mechanism is not fully clear, but significant research effort has been devoted to understand the function of this protein. The sudden interest on this protein was generated when two almost simultaneously published articles reported the identification of its viral restriction function and Vpu's antagonistic role against BST-2 (Van Damme 2008, Neil 1008). In summary, when cells are transfected with wildtype HIV-1 genome, the mature virions is able to bud from the cell surface normally, and BST-2 level is down-regulated. When the vpu gene is deleted from the genome, heavy aggregation of the virus particles is observed on the cell surface as direct result of the co-expression of BST-2. Therefore, it is theorized that there is direct interaction between Vpu and BST-2, and further research reveal more evidence and details on this interaction. One important characteristic is that the interaction is localized to the TM domains of the two proteins from various mutagenesis studies (McNatt 2009). BST-2 has very unique secondary structure features which include a short N-terminal cytoplasmic tail, a single transmembrane helix, a coiled-coil

ectodomain and a C-terminal glycosyl-phosphatidylinositol GPI anchor which is added on during post-translational modification. The native protein is found to be a homo-dimer stabilized mainly by select residues in the ectodomain, and maintaining the dimerization conformation is important for the biological function (Perez-Caballero 2009).

There are several important aspects of the interaction between Vpu and BST-2 that need to be elucidated. Firstly, the evidence for the direct interaction of Vpu and BST-2 is scarce if at all because the studies have mostly been done within cellular environment. Secondly, more molecular level details are needed to fully understand how the two proteins interact with each other and develop structural models for the complex. As a collaborative effort with Dr. John Guatelli's group at the department of medicine at UCSD, we investigated this interaction by approaching it at both cellular and molecular level. Unless otherwise stated, all of the biological experiments involving human cell lines and expression levels are performed by members of Guatelli group, and their experiments uses mutagenesis approach to reveal important residues involved in the antagonism interaction at the cellular level. For molecular level studies, solution and solid-state NMR techniques are used to gain high resolution information on the protein-protein interaction under micelle or bicelle environment. For this approach, an construct of the BST-2 TM domain is made using residues 18 to 47 from the human BST-2 sequence with five more extra lysines at the C-terminus as solubilization tag. One mutation is introduced where Cys20 is mutated to serine to

prevent problems with protein aggregation due disulfide bonds. The full sequence of the BST-2 TM construct is shown below.

KRSKLLLGIGILVLLIIVILGVPLIIFTIKKKKKK

4.2 Material and Methods

The expression and purification procedures for BST-2 are the same as for Vpu described in Chapter 2. For the paramagnetic relaxation enhancement (PRE) experiments, the spin label MTSL was purchased from Toronto Research Chemicals. MTSL was added to proteins dissolved in SDS and reduced DTT (Sigma), and the solution was incubated at room temperature overnight. Excess MTSL was removed using Sephadex G-25 Quick Spin Protein Columns (Roche Diagnostic). SDS and residual free MTSL were removed by extensive dialysis. Solution and solid-state NMR sample preparation and spectroscopic experiments were the same as previously described in Chapter 2. The structure calculation was performed using a simulated annealing protocol in Xplor-NIH (Schwieters 2002) the temperature cooled from 3000K to 25K in setps of 12.5K with experimentally determined RDC values as constraints. The structure is the average of 10 structures-ensemble and displayed by MolMol (Koradi 1996). The docking calculation was performed using Rosetta 3.1 (Gray 2003) with the NMR structures of Vpu TM and BST-2 TM. The two structures were allowed to assemble from an initial distance of 8 Å apart, keeping the backbone rigid while varying the rotation of the helices and side-chains. A total of 5000 docking

poses were search during the calculation. Structures of the Vpu-BST-2 complex were displayed by Chimera (Pettersen, 2004).

4.3 Structural Characterization of BST-2

The 3D structure of the coiled-coil ectodomain of BST-2 was determined by X-ray crystallography (Yang 2010), but there is no high-resolution structure characterization on the TM domain. SDS-PAGE of the purified BST-2 TM construct roughly corresponds to that of a dimer which is the predicted oligomerization state of the native protein. This indicates that ectodomain is not required for the dimerization of the TM domain. Solution NMR provides a quick way to identify the secondary structural features of protein in micelle. HSQC spectrum of the ^{15}N uniformly labeled BST-2 TM solubilized in 100mM DHPC at pH4 is shown in Fig4.1A. The peaks are well resolved, and the full backbone assignment including amides and alpha carbon is made though analysis of 3D experiments and confirmed by selectively labeled samples. The residual dipolar coupling (RDC) values for each amide is obtained under stretched polyacrylamide gel condition. The resulting values are plotted against the residue number and shown in Fig4.1B. Based on the dipolar wave fitting, the transmembrane helix spans from residues 24 to 45 with a proline induced kink at residue 40. This is evident from the fitting of the two dipolar waves that are different in the magnitude range but not in the phase. This confirms that this sequence predicted to be the TM domain of BST-2 is indeed a helical structure. The dihedral angle

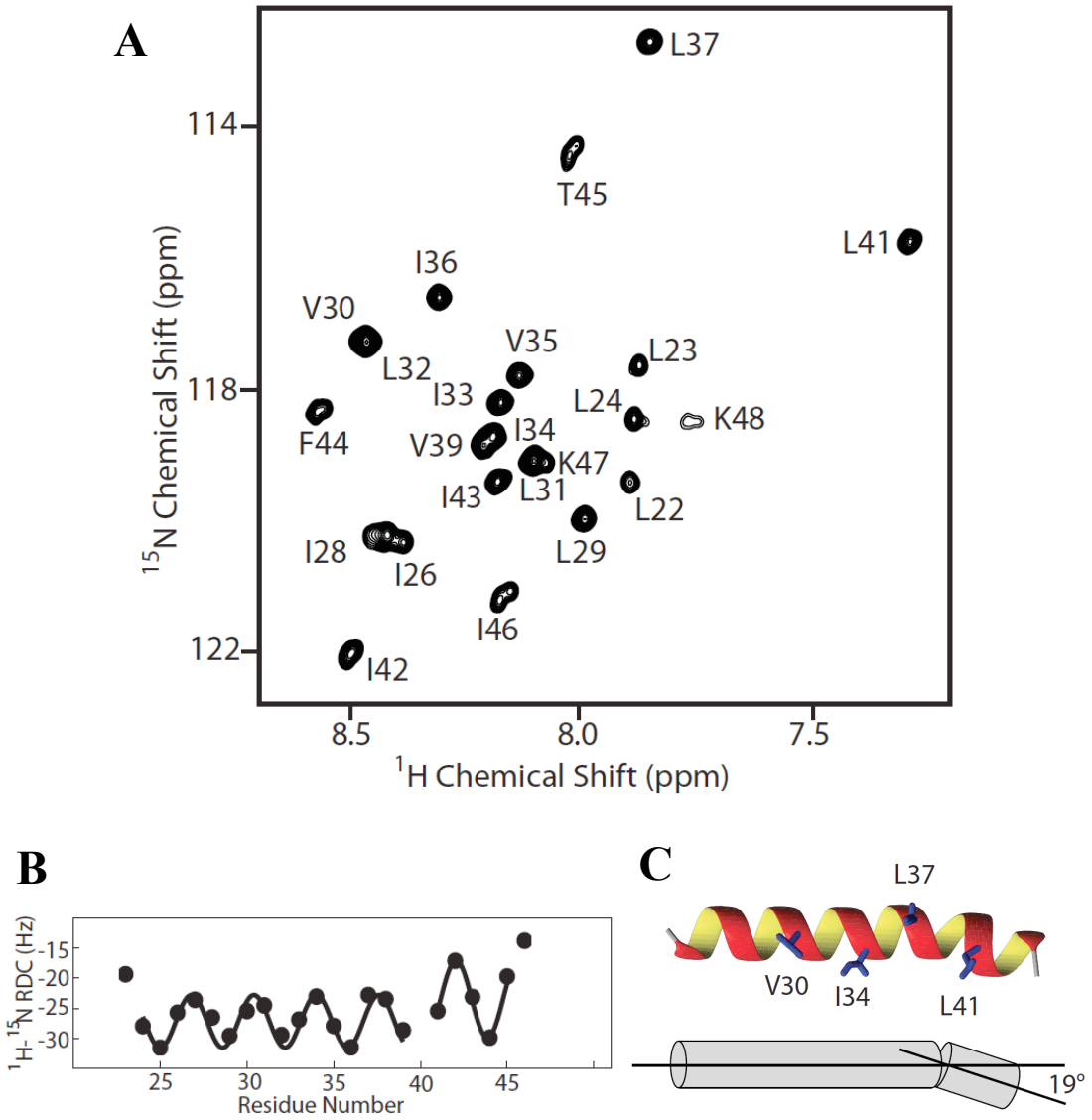

Figure 4.1: Characterization of BST-2 TM by solution NMR. A) HSQC of BST-2 TM in DHPC micelle at pH7.4 and 37°C. The full resonance assignment is achieved through triple-resonance HNCA and HN(CO)CA correlation experiments. B) Dipolar wave fitting of the BST-2 TM backbone amide RDC values obtained sample partially aligned in stresssed gel. Presence of a kink at residue P40 is indicated by the break in the fitting. C) Average backbone structure from 10 structure ensemble calculated from RDC restraints using Xplor-NIH. Backbone RMSD is 1.9Å, and the kink is averaged at 19°.

predicted from chemical shift values using TALOS (Cornilescu 1999) and RDC values are utilized to calculate the 3D backbone structure of BST-2 TM. The average of the 20 structure ensemble calculated using the annealing protocol form Xplor-NIH (Schwieters 2002) is shown in Fig4.1C. The backbone RMSD is around 1.2Å. The kink at residue 40 is averaged to around 19° which is falls to the expected range for proline induced kinks for membrane proteins (Senes 2004). The indicated residues with the side-chain highlighted are found to be important in the interaction with Vpu as will be discussed in the following sections.

For the study within a bilayer environment, BST-2 TM is incorporated into bicelles and studied using solid-state NMR studies. The 1D and 2D solid-state spectrum is shown in Fig4.2 A and B, respectively. The 1D ^{15}N chemical shift spectrum shows that the sample is well-aligned within the magnetic field as there is no

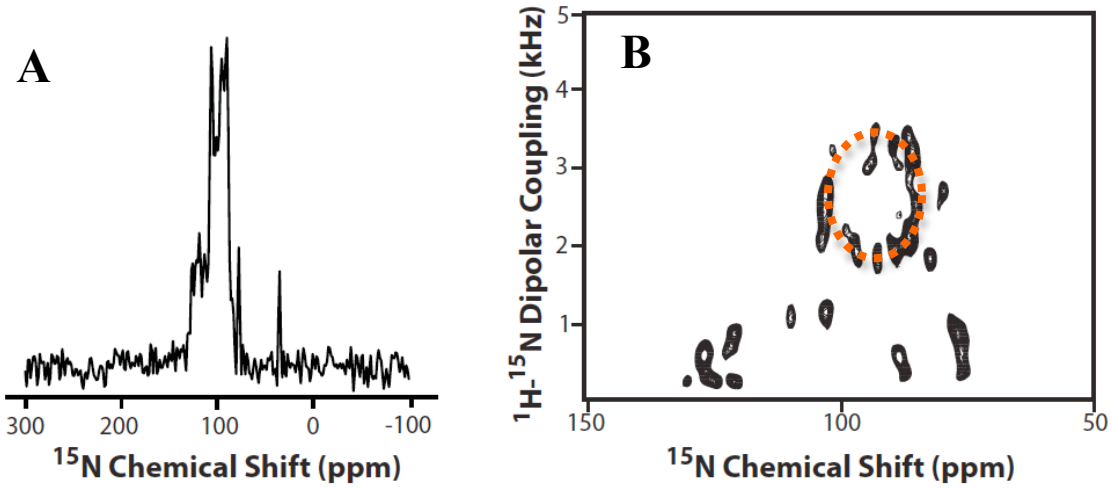

Figure 4.2: 1D and 2D solid-state spectra of BST-2 TM in magnetically aligned bicelle. A) 1D ^{15}N chemical shift spectrum of uniformly labeled BST-2 TM from ^{1}H-^{15}N cross polarization experiment. B) 2D ^{15}N chemical shift/^{1}H-^{15}N dipolar coupling spectrum of the same sample. PISA wheel fitting is shown as the dashed ellipse and helix tilt is approximately 19° determined from the fitting.

evidence of powder pattern. The 2D spectrum is shown with the PISA wheel fitting represented with dashed ellipse. The resonances are well resolved and can be fitted with a single wheel, and this is a confirmation that BST-2 TM is a stable helix within the bilayer. The helix tilt angle for the construct is 21° based on the best fitting, so it is about 9° smaller in comparison to the wildtype Vpu-TM. This suggests that BST-2 and Vpu would interact with each other with a slightly crossed conformation, at least at the initial contact stage. As evidenced by the single PISA wheel fitting, the signals around the fitting most like comes from the helical region of residues 24 to 39. It is likely that the rest of signals come from the second part (residues 41-45) of the kinked helix, but resonance assignment is needed to confirm that. Overall, the results have confirmed the helical secondary structure of the BST-2 TM with high resolution detail. Additionally, the length of the helical region and the presence of a kink are identified.

In order to determine the rotation angle of the BST-2 helix within the bilayer, 2D spectrum is recorded on a selectively ^{15}N labeled valine BST-2 sample as shown in Fig4.3A (red). Valine is chosen because there are three valine residues, and one of them places far apart from the other two on the ideal helical wheel, so this enables a quick discernment of the relative positions of the residues. The spectrum shows a clear expected distribution of a single peak which corresponds to V30 and two aggregated peaks which correspond to V35 and V39. The rotation of the helical wheel can then be determined and is shown in Fig4.3B.

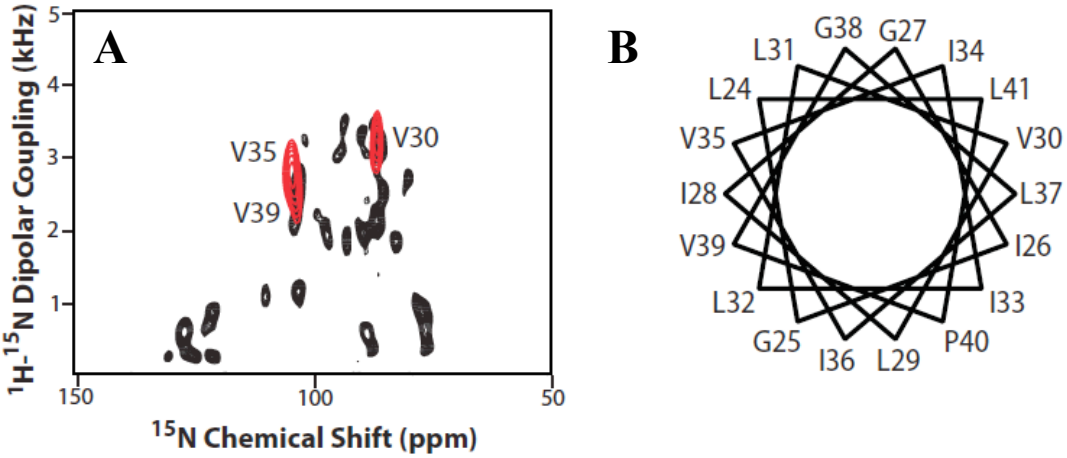

Figure 4.3: BST-2 helical wheel rotation determined from selective ^{15}N labeled Val sample. A) 2D ^{15}N chemical shift/^{1}H-^{15}N dipolar coupling spectrum of ^{15}N valine BST-2 sample (red) in magnetically aligned bicelle is superimposed on that of the uniformly labeled sample (black). The assignment is based comparison to the ideal helical wheel representation of the BST-2 TM shown in B).

4.4 Solution NMR Study of Vpu-BST-2 Interaction

The potential interaction between Vpu and BST-2 are first characterized using solution NMR because its high resolution allows for the monitoring of individual residues. The basic protocol for studying protein-protein interaction is recording the chemical shift differences between a ^{15}N labeled protein in the absence and presence of the unlabeled protein binding partner. The residues showing the largest differences would likely to be important for the interaction. The reversal experiment is then carried out on the ^{15}N labeled partner protein to identify its important residues. When the experiment is done with BST-2 TM and Vpu-full length (FL) constructs, results show strong evidence that these two proteins have an affinity for each other. Fig4.4 shows the comparison of 1D and 2D HSQC spectra of the BST2-TM with and without unlabeled Vpu-FL in a approximately 1:1 molar ratio at pH7.4 in 100mM DHPC. The

1D spectrum (Fig4.4A) shows a severe loss of overall intensity and resolution of the peaks in the case of BST-2 with Vpu-FL (bottom) when compared to the spectrum of BST-2 alone(top), and this is a typical sign of sample aggregation as the increase in molecular weight results in the increase in the relaxation rate thus broadening the linewidth of the peaks. This is the first observed evidence for direct protein-protein interaction between Vpu and BST-2 as introducing the two proteins in the same environment promoted aggregation. The interaction appears to be strong as prolonged

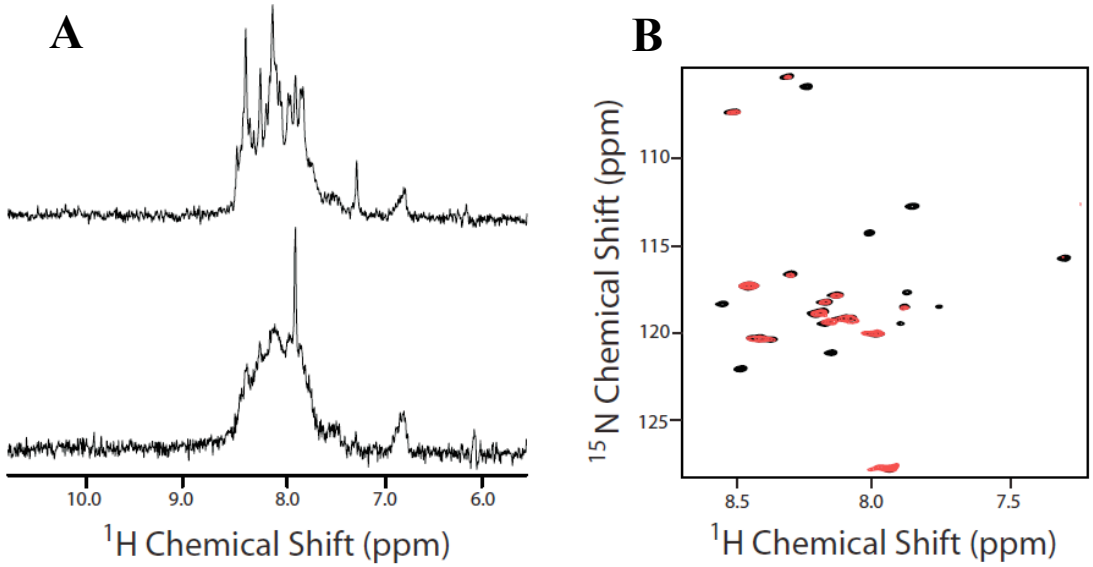

Figure 4.4: Interaction between Vpu full length and BST-2 TM in micelle. A) Comparison of 1D chemical shift spectrum of 15N uniformly labeled BST-2 TM alone (top) and with 1 molar equivalent of unlabeled Vpu full length (bottom) in DHPC at pH 7.4. Significant line broadening is observed indicating the presence of aggregation. B) 2D HSQC spectrum of BST-2 TM with unlabeled Vpu full length. Several peaks have broadened beyond detection while others still have low but visible intensity suggesting certain degree of internal motion still exists for those residues.

sample (> 3 hours) incubation or additional unlabeled Vpu-FL induces protein precipitation. The overlay of 2D spectra (Fig4.4B) provide additional look at any

differential line broadening effect among individual residues. More than half of the peaks are broadened beyond detection indicating a server loss of dynamics. The rest of the peaks correspond to residues that have some degree of internal motion that allow them to have relatively stronger intensities, and they are mainly located in the region between residues 25 and 35, or the N-terminal half of the helix.

The BST-2 TM and Vpu-FL pairing gave very important preliminary insights into the interaction, but the presence of aggregation and precipitation make it challenging for high resolution characterization of the complex. The problem is resolved by substituting Vpu-FL with Vpu-TM as the TM construct is relatively more stable and have higher solubility. The resulting overlay of the ^{15}N BST-2 spectra with (red) and without (black) unlabeled Vpu-TM in 1:4 BST:Vpu molar ratio is shown in Fig4.5A. There is no overall decrease of the intensity or resolution, and the amount of Vpu-TM can reach up to 5-fold excess of BST-2 TM. The Vpu-TM induced chemical shift difference of BST-2 TM is plotted against residue number and shown in Fig4.5C. The magnitude of the difference is relatively small in comparison to typical protein-protein interactions for soluble proteins. This is an indication that the interaction is weak, and this is somewhat expected as the experiment is done in a micelle condition. It is likely to be energetically more favorable for a protein to be incorporated alone into the micelle environment rather to be incorporated as a complex as it creates a disturbance for the hydrophobic core of the micelle. Therefore, there is an energy barrier for one protein to escape ones surrounding lipids and move into the lipids of another protein in order for the binding interaction to happen. This also introduces the

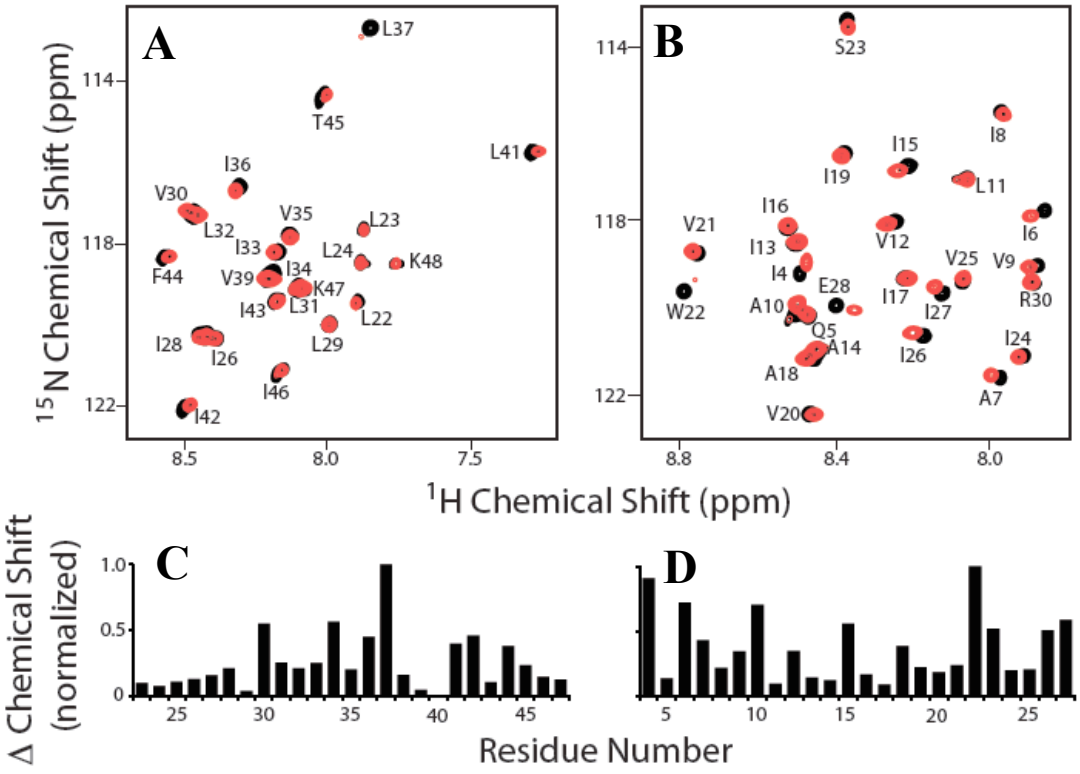

Figure 4.5: Interaction between BST-2 TM and Vpu TM in micelle. A) HSQC spectrum of ^{15}N uniformly labeled BST-2 in the absence (black) and presence of 4 molar excess of unlabeled Vpu TM. B) HSQC spectrum of ^{15}N uniformly labeled Vpu TM in the absence (black) and presence of 4 molar excess of unlabeled BST-2 TM. C) Chemical shift difference plot for BST-2 calculated from spectra in A). D) Chemical shift difference plot for Vpu calculated from spectra in B).

possibility that there is a chemical exchange rate that affect the final averaged spectrum. Nevertheless, the plot does indicate certain residues that have higher chemical shift differences than the others. Specifically, residues 30, 34, and 37 stand out and this suggests that they may have important roles in the interaction. In addition to the chemical shift change, there is a dramatic reduction (~50%) in the intensities of the residues 37 and 41, so it suggests that these two residues become relatively more rigidified as result of the interaction. Overall, the residues that display the biggest change in chemical shift and/or intensities are lined up on the same face of the helix, so this is a strong indication that this face of the BST-2 TM is the one that binds to Vpu-TM.

The reverse experiment is performed on ^{15}N labeled Vpu-TM, and the resulting overlay of the spectra with (red) and without (black) the unlabeled BST-2 TM and the corresponding chemical shift difference plot are shown in Fig4.5B and D, respectively. As similar to the BST-2 result, the unlabeled protein partner induced small but detectable chemical shift changes associated with a number of residues. The specific residues that experienced more pronounced perturbation include 4, 6, 10, 15, and 22, and W22 has very significant decrease in peak intensity due to line broadening indicating an increase in its rigidity. Unlike the case of BST-2, the perturbed residues do not all localize to a particular face of the helix, but there is a small preference towards the face occupied by 6, 10, and 22. For W22, its decrease in peak intensity may come from its bulky hydrophobic side-chain being locked into a particular space of the BST-2 TM.

An important question regarding the interaction is the conformation state of the complex, and there are basically three possibilities: parallel, anti-parallel, and crossed/perpendicular. It should be noted that these are not strictly defined by the geometric standards, but rather rough relative positions of the N and C termini of the two proteins. The crossed conformation can be ruled out because it would be energetically unfavorable considering the interaction occurs within a lipid bilayer environment, and the previously described solid-state NMR results show that there is only a small difference (~9°) in the tilt angle between the two proteins. Therefore, it would be unfeasible for the proteins to undergo dramatic reorientation within the bilayer to form a crossed conformation in which the termini of the two helices are far apart from each other. In addition, the chemical shift perturbation result show that the residues affected by the interaction are located throughout the length of the helices suggesting that the binding site(s) is not limited to a single point on the helices. Vpu is a type I integral membrane protein, and BST-2 is type II, so the two proteins are expected to be incorporated into the membrane as anti-parallel conformation relative to each other. In order to confirm this, inter-molecular distance information is needed for specific residues on the two proteins. This is particularly challenging since the interaction is weak and involves the possibility of certain on-off rate, so the conventional NOE based experiments would not be successfully applied to the sample. The reason again involves the fast decay of signal, and the problem is resolved by using paramagnetic spin labels as this method is more sensitive and covers larger distance (up to 30Å) as explained in Chapter 1. Cysteine is introduced into the Vpu-

TM construct by mutating residue Q5 to provide an attachment site for the paramagnetic label, MTSL. After covalently linking MTSL to Vpu-TM Q5C (not isotopically labeled), the modified protein is added to ^{15}N labeled BST-2 TM, and the resulting change in the HSQC peak intensity due to paramagnetic line broadening is shown in Fig4.6A. Residues C-terminal of 46 shows increasing reduction in the peak intensity, and the observed magnitude of reduction is as much as 50% in the case of

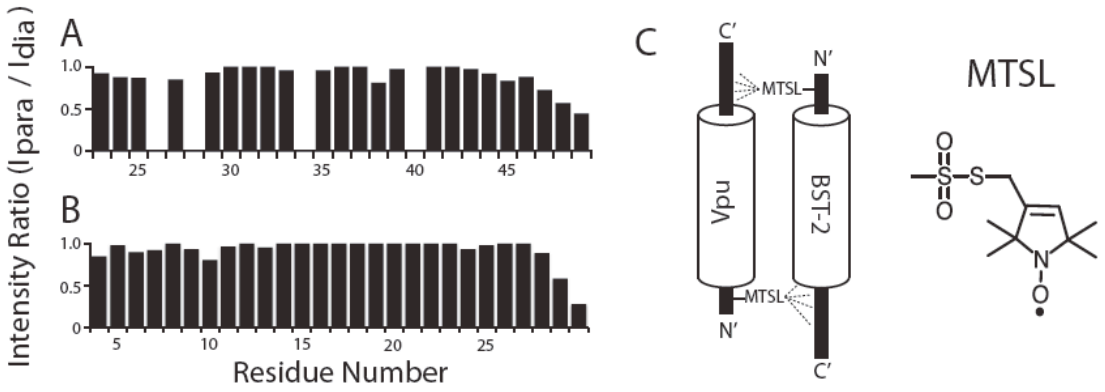

Figure 4.6: Characterization of the BST-2 Vpu interaction in micelle by PRE. A) HSQC intensity change of ^{15}N labeled BST-2 induced by unlabeled Vpu with a MTSL spin labeled attached to the N-terminal region. B) A) HSQC intensity change of ^{15}N labeled Vpu induced by unlabeled BST-2 with a MTSL spin labeled attached to the N-terminal region. I_{para} is the peak intensity when the spin label is in the paramagnetic state, and I_{dia} is the peak intensity when the spin label is reduced by excess amount of ascorbic acid. Since the spin-label placed on the N-terminal region of one protein affects only the C-terminal region of the other, it is likely that the interaction involves a anti-parallel conformation as depicted in the schematic diagram in C). The structure of MTSL is shown next to it.

residue 49 while the residues after 49 are not observable due to D_2O exchange effect. The result supports the anti-parallel conformation since the paramagnetic label is placed on the N-terminal side of Vpu-TM, and it affects the residues on the C-terminal region of BST-2 TM. To further confirm the finding, spin label is added to a BST-2 TM construct where Serine20 is mutated to cysteine since the wildtype sequence is a

cysteine at that site. The HSQC peak intensity change on the ^{15}N labeled Vpu in the presence BST2-MTSL is shown in Fig4.6B, and the result indicates that the C-terminal residues of Vpu, particularly the ones after residue 28, are significantly affected by the paramagnetic labeled placed on the N-terminal region of BST-2. Therefore, the results are consistent in supporting the anti-parallel conformation of the interaction within the micelle as summarized in the schematic diagram shown in Fig 4.6C. It provides strong and direct evidence for validating the model derived from biological properties.

The preliminary solution NMR data gave valuable insights into the potentially important interacting residues and surfaces. However, one may raise the question of whether the observed interactions are specific or just non-specific interactions that have little or no biological relevance. In order to address the question, we used a mutant Vpu-TM that was found to be defective in facilitating virus release and down-regulating BST-2 in cell assays. The mutant has three of the alanines (A10, 14, and 18) mutated the phenylalanine, and it will be referred as Vpu-A3XF mutant for the remainder of the thesis. The reason for the initial mutation was that the alanines are on the same face of the helix and hypothesized to be important in helical interactions as the small side-chains provide insertion space for bulky side-chains of the binding partner. This mechanism is coined as the GAS motif for the roles of residues with small side-chains (Senes 2004). After the unlabeled Vpu-A3XF mutant is added to the ^{15}N labeled BST-2 TM at a four fold molar excess, the resulting HSQC spectrum shows very little change in comparison to that of BST-2 alone. The most telling

evidence is the overall lack of chemical shift change except for the small change with residue L23 located on the N-terminal region. In addition, the dramatic decrease in the intensity of L37 due to line broadening is no longer presence. This is a clear indication that the two constructs have little or no binding interaction, so the result is supportive of biological results, and the Vpu A3XF mutant serves as a good negative control for the experiment.

4.5 Solid-State NMR Study of Vpu-BST-2 Interaction

In order to characterize the interaction in a bilayer environment, solid-state NMR is employed to examine the constructs in magnetically aligned bicelle. There are several areas of interest that need to be addressed. First of all, we want to investigate any significant structural change such as distortion of the helix resulting from the interaction. Secondly, we want to see if there are any topological changes such as helix tilt and rotation changes. Fig4.7 shows the 2D ^{15}N chemical shift ^{1}H-^{15}N dipolar coupling spectra of the ^{15}N labeled protein with (Red) and without (Black) the binding partner. In the case of labeled BST-2 with unlabeled Vpu (Fig4.7A), two important features arise from the comparison. Firstly, the presence of Vpu induced a small shift of the BST-2 wheel pattern towards the lower dipolar coupling and higher chemical shift region. As the result, the new PISA wheel fitting puts the helix tilt angle at 24° degrees, 3° larger than BST-2 alone. Secondly, the overall resolution of the spectrum has decreased as displayed by the broadening of the peaks, and this suggests an overall increased dynamics and destabilization of the protein within the bilayer. There is no

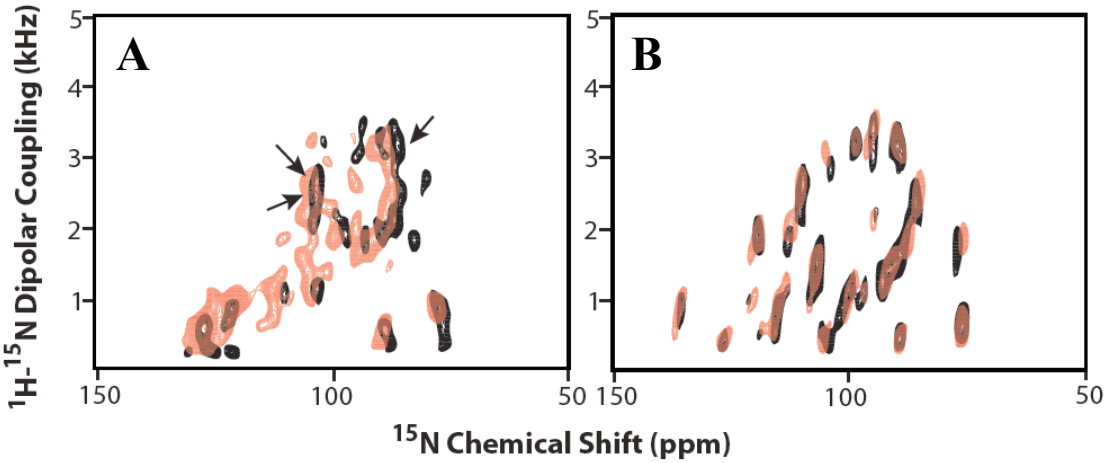

Figure 4.7: Interaction between BST-2 and Vpu in magnetically aligned bicelle characterized by solid-state NMR. A) 2D ^{15}N chemical shift/^{1}H-^{15}N dipolar coupling spectrum of BST-2 TM in absence (black) and presence (red) of unlabeled Vpu TM. B) 2D ^{15}N chemical shift/H-N dipolar coupling spectrum of Vpu TM in absence (black) and presence (red) of unlabeled BST-2 TM.

significant change in the pattern of the peaks, and spectrum can still be fitted with one PISA wheel, so there is no large distortion to the structure BST-2 in the presence Vpu.

On the Vpu side, its spectra with and without unlabeled BST-2 (Fig4.7B) is essentially the same. The peaks overlap very well, and there is no change in the resolution or linewidths of the peaks. This shows that the structure, topology, and stability of Vpu are not affected by the presence of BST-2. It is possible that the tryptophan residue plays a role in the stability of Vpu as it has been shown to have anchorage effect on the transmembrane peptide (Planque 2003). This is supported by the results described in Chapter 3 on destabilizing effect of mutating tryptophan of M2 to alanine within the bilayer. The stability of Vpu within the bilayer may be important in the down-regulation of BST-2 and even CD4 receptor in that Vpu itself escape the process of being subjected to the proteosome degradation pathway. The solid-state

results on the interaction suggest that Vpu and BST-2 maintain their intra-molecular structural features during the contact, but BST-2 tilt its helix within bilayer towards Vpu while Vpu maintains its tilt angle. As the difference in the spectral resolution suggests, this introduce the possibility of a 'wobble' motion to BST-2 while Vpu serves as a rigid anchor pole for the complex conformation.

One issue that still needs to be addressed is the discrepancy regarding BST-2 ΔLG T45I mutant which was found to be non-responsive to Vpu in biological assays but induced the same chemical shift perturbation profile for Vpu-TM as the wildtype BST-2 TM did in micelle by solution NMR. One hypothesis is that the deletion of the two residues, LG, in the TM domain would have significant effect on the tilt angle of the helix and thus have an impact on the proper binding interaction. 2D solid-state

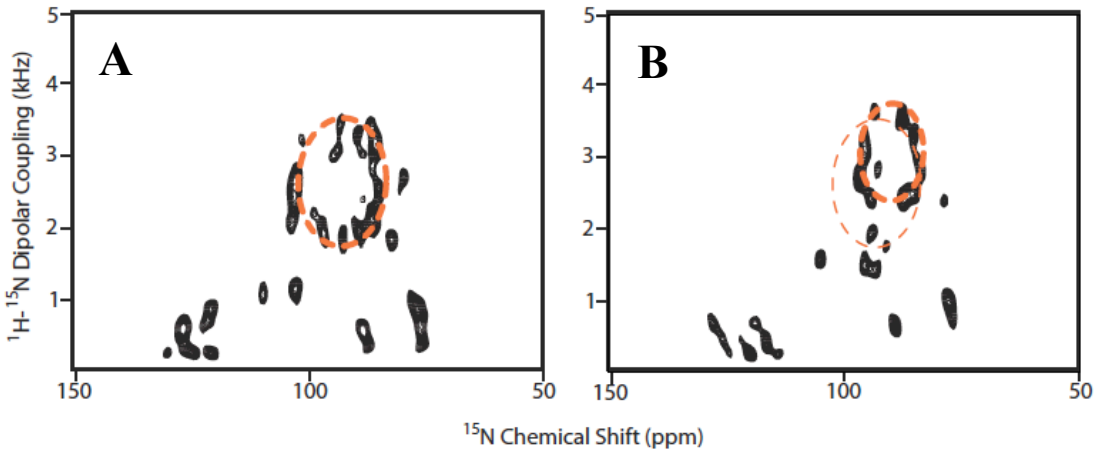

Figure 4.8: Comparison between wt BST-2 TM and BST-2 TM ΔLG T45I mutant in bicelles. A) 2D ^{15}N chemical shift/H-N dipolar coupling spectrum of wt BST-2 TM in bicelle. Its helix tilt angle is estimated to be 21° from the PISA wheel fitting (dashed ellipse). B) 2D ^{15}N chemical shift/H-N dipolar coupling spectrum of BST-2 TM ΔLG T45I mutant and its tilt angle is 15° in comparison to the wildtype PISA wheel shown as the thinner ellipse.

NMR spectrum is recorded for the mutant in bicelle and is shown in Fig4.8B. The PISA wheel fitting indicates that the tilt is around 15°, 6° smaller than the wildtype BST-2 TM whose PISA wheel is superimposed as the thinner ellipse. This difference confirms the difference in tilt and provides a possible explanation for the discrepancy. As shown in the bilayer interaction, BST-2 appears to be tilting towards Vpu upon binding, so the optimal relative tilt between Vpu and BST-2 may be important for the binding to occur. In the case of BST-2 ΔLG T45I mutant, its tilt is significantly different from the wildtype and may not be able to position itself in the proper conformation to interact with Vpu within the bilayer. However, in a micelle environment, the protein does not have the tilt restriction as the hydrophobic environment is more malleable than that of a bilayer, so the mutant has the freedom to move into the optimal binding conformation with Vpu. It is still unclear the significance regarding the T45I mutation as it should not have impact on the tilt angle. It is possible that it affects the binding surface of the complex in terms steric hindrance and/or hydrogen bonding as it replaces a polar residue with a bulky hydrophobic one and T45 is located on the face of the helix found to be important in the interaction by solution NMR.

4.6 Biological Study of Vpu-BST-2 Interaction

As part of the collaborative effort on this project, members of Prof. John Guatelli's group performed cellular and molecular biology experiments that not only provided guidance on the key aims for designing NMR experiments but also the

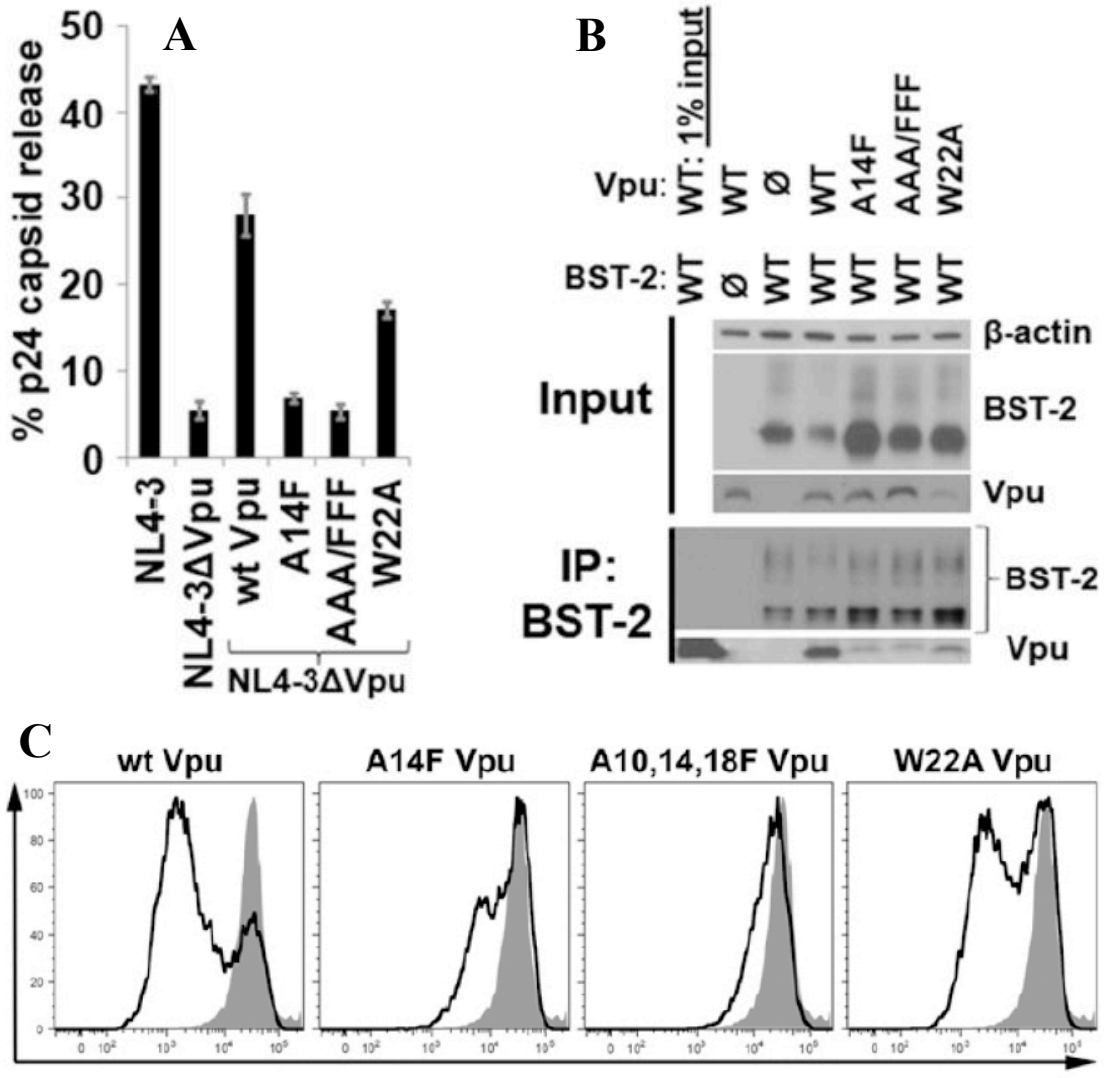

Figure 4.9: Biological characterization of the effects of Vpu mutations on the interaction in human cells. A) Percent of viral capsid release with respect to total virus production from cells expressing various constructs of Vpu. NL4-3 is the HIV-1 viral genome, and NL4-3ΔVpu is the genome with the vpu gene deleted. Mutant Vpu gene is introduced artificially by transfection to cells expressing NL4-3ΔVpu. B) Immunoprecipitation of BST-2 showing the wildtype Vpu was able to be co-immunoprecipitated while the defective Vpu mutants have significant reduced level of binding. C) Surface BST-2 down-regulation by wildtype or mutants of Vpu measured by monitoring the GFP expression (a tranfection marker) with flow cytometry.

validation for the conclusions drawn from the NMR characterization. This section will briefly describe the methods and results from these biological studies. The interaction between the wildtype and mutant forms BST-2 and Vpu is evaluated by monitoring the surface BST-2 down-regulation and fractional viral capsid release in human cells. Cellular protein-protein interaction is studied by co-immunoprecipitation, and the expression of specific construct is confirmed with immuno blot. On the Vpu side, the percent capsid release is significantly when the cells express a viral genome that does not contain the vpu gene (NL4-3ΔVpu) in comparison to the expression of a normal viral genome as shown in Fig4.9A. The importance of specific residues on the TM of Vpu is tested by an alanine scanning mutagenesis approach. Results show that the Vpu W22A mutant is a moderately defective mutant and the Vpu AAA/FFF (A3XF) and A14F mutants reduce the capsid release level to the same as that in the absence of Vpu. The flow cytometry results shown in Fig4.9C indicate that A14F and A3XF mutants and to a lesser extend the W22A are defective in the down-regulation of the BST-2 from the cell surface in comparison to wildtype. Furthermore, the Vpu mutants interacted poorly inside the cell as indicated from the results of co-immunoprcipitation of BST-2 shown in Fig4.9B. Overall, the results give strong evidence for importance of the A10, 14, 18 and W22 residues of Vpu in the protein-protein interaction with BST-2. In addition, all of the defective Vpu mutants are active in the CD-4 down-regulation confirming that the Vpu-BST-2 interaction is localized mostly in the transmembrane domain.

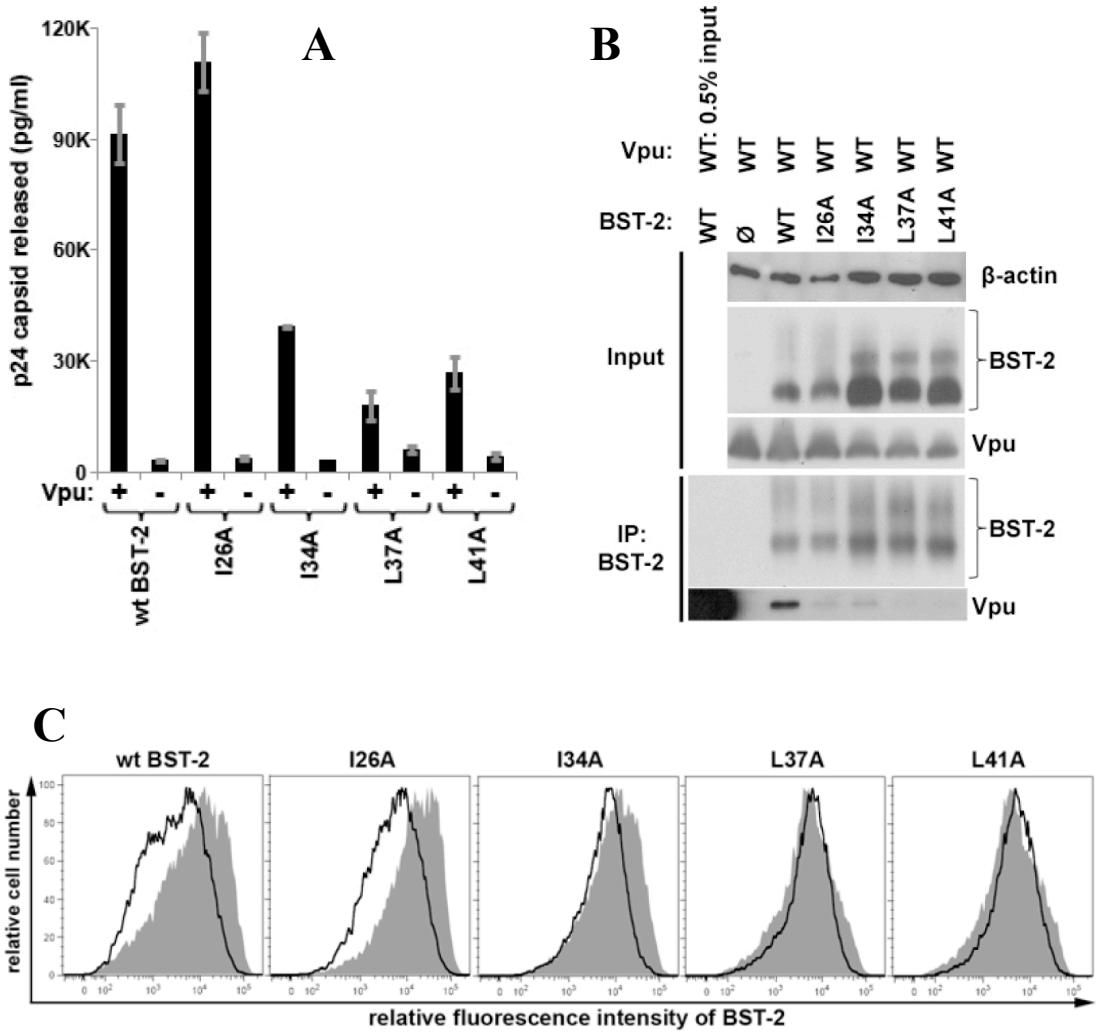

Figure 4.10: Biological characterization of effects of BST-2 mutations on the interaction in human cells. A) Percent of viral capsid release with respect to total virus production from cells expressing various constructs of BST-2 in presence and absence of Vpu expression. B) Immunoprecipitation of BST-2 from cells C) Surface BST-2 (wildtype or mutant) down-regulation by Vpu measured by monitoring the GFP expression (a tranfection marker) with flow cytometry.

On the BST-2 side, the same experiments are performed to confirm the importance of specific residues in the interaction deduced from the NMR experiments. As described in section 4.4, residues 34, 37, and 41 of BST-2 are found to be most perturbed in the solution NMR experiment. For wildtype BST-2, it is able to restrict the release of viral capsid in the absence of Vpu but unable to do so in the presence of Vpu as shown in Fig4.10A. However, when I34A, L37A, and l41A mutants of BST-2 are found to still be able to restrict the viral release in the presence Vpu, though not at the same level as that in the absence of Vpu. As a control, residue I26 of BST-2 which is not perturbed in the NMR experiment is mutated to alanine and the mutant is found to behave the same as the wildtype. The flow cytometry results in Fig4.10C show that the I34A, L37A, and l41A mutants of BST-2 are not down-regulated by Vpu, and the immunoprecipitation data (Fig4.10B) shows they interact poorly with Vpu in cell. Another defective mutant of BST-2, ΔLGT45I is found be the most defective in responding to Vpu as indicated by the viral release results shown in Fig4.11A, and the ΔLG mutation alone produced a impaired response, but to a lesser extend, and both mutants are unable to be down-regulated by Vpu as indicated by results shown in Fig4.11B. This introduced the interesting dilemma when solution NMR shows the ΔLGT45I mutant has the same perturbation pattern as that of wildtype BST-2, and promoted the investigation of its tilt angle in the bilayer. As shown in section 4.5, the BST-2 mutant has a helix tilt 6° smaller than the wildtype, and this could serve as the possible explanation for the dilemma as the mutant does not have enough freedom in the bilayer to move into the favorable binding conformation.

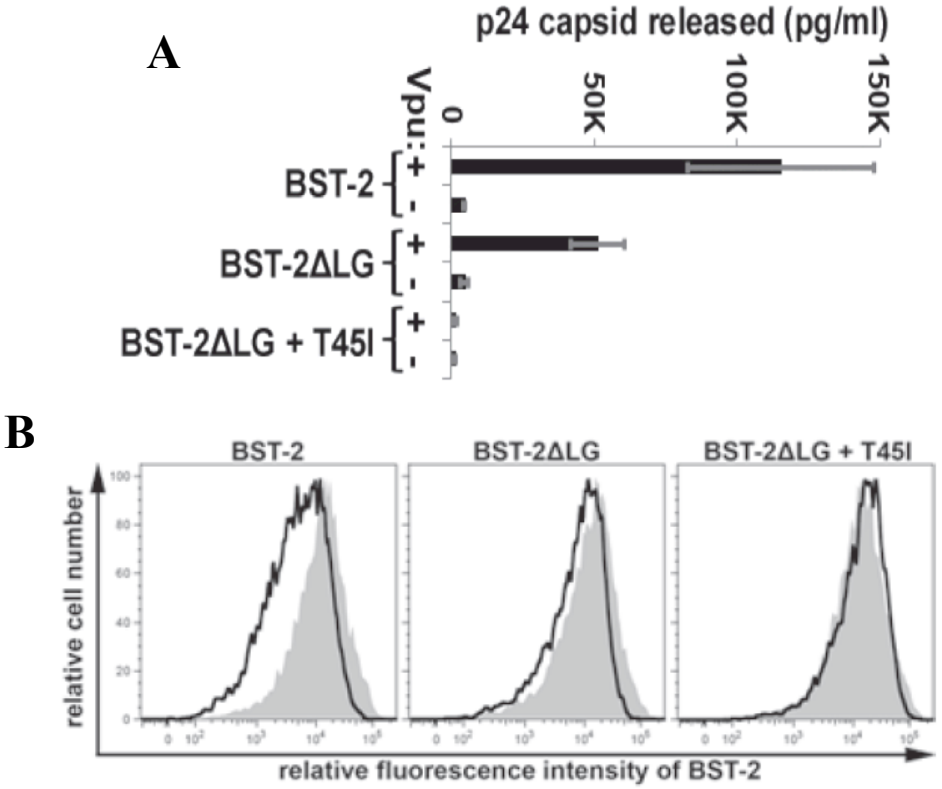

Figure 4.11: Biological characterization of ΔLG and ΔLGT45I mutants of BST-2. A) Percent of viral capsid release with respect to total virus production from cells expressing various constructs of BST-2 in presence and absence of Vpu expression. B) Surface BST-2 (wildtype or mutants) down-regulation by Vpu measured by monitoring the GFP expression (a tranfection marker) with flow cytometry.

4.7 Computational Modeling of the Vpu-BST-2 Complex

The combination of spectroscopic and biological results gave important insights into the molecular nature of the binding interaction. In order to test whether the proposed conformation of the complex is energetically favorable, a docking simulation is performed on the experimentally determined structures of Vpu and BST-2 using Rosetta 3.1. The two structures are initially placed 8Å apart and then allowed to come to contact with each other. The backbone structures were kept rigid and Vpu is kept in place while the rotation and tilt angles of BST-2 helix and side-chains were allowed to vary to find the optimal binding conformation. Twenty lowest energy complexes were selected out of 5000 calculated poses, and they converge well as indicated by the backbone root means square deviation (RMSD) of 2Å. The 20 structures ensemble of BST-2 as a complex with Vpu is shown in Fig4.12A, and the lowest energy pair is show in Fig4.12B with selective side-chains of Vpu colored in red and side chains of BST-2 colored in blue. Results shows good agreement with the experimental data as the face lined with residues 10, 14, 18, and 22 of Vpu is binding with face of BST-2 lined with residues 30, 34, 37, and 41. The bulky side-chains of leucines and isoleucines of BST-2 fit into the gaps created by the alanine side-chains Vpu, and the side-chain W22 of Vpu is seen as within a rigid confinement between the two proteins. The helices are paired in an anti-parallel fashion with slight difference in the relative tilt of the axes. In comparison, when the same docking simulation is performed on BST-2 and Vpu A3XF mutant, the complex does not converge well as

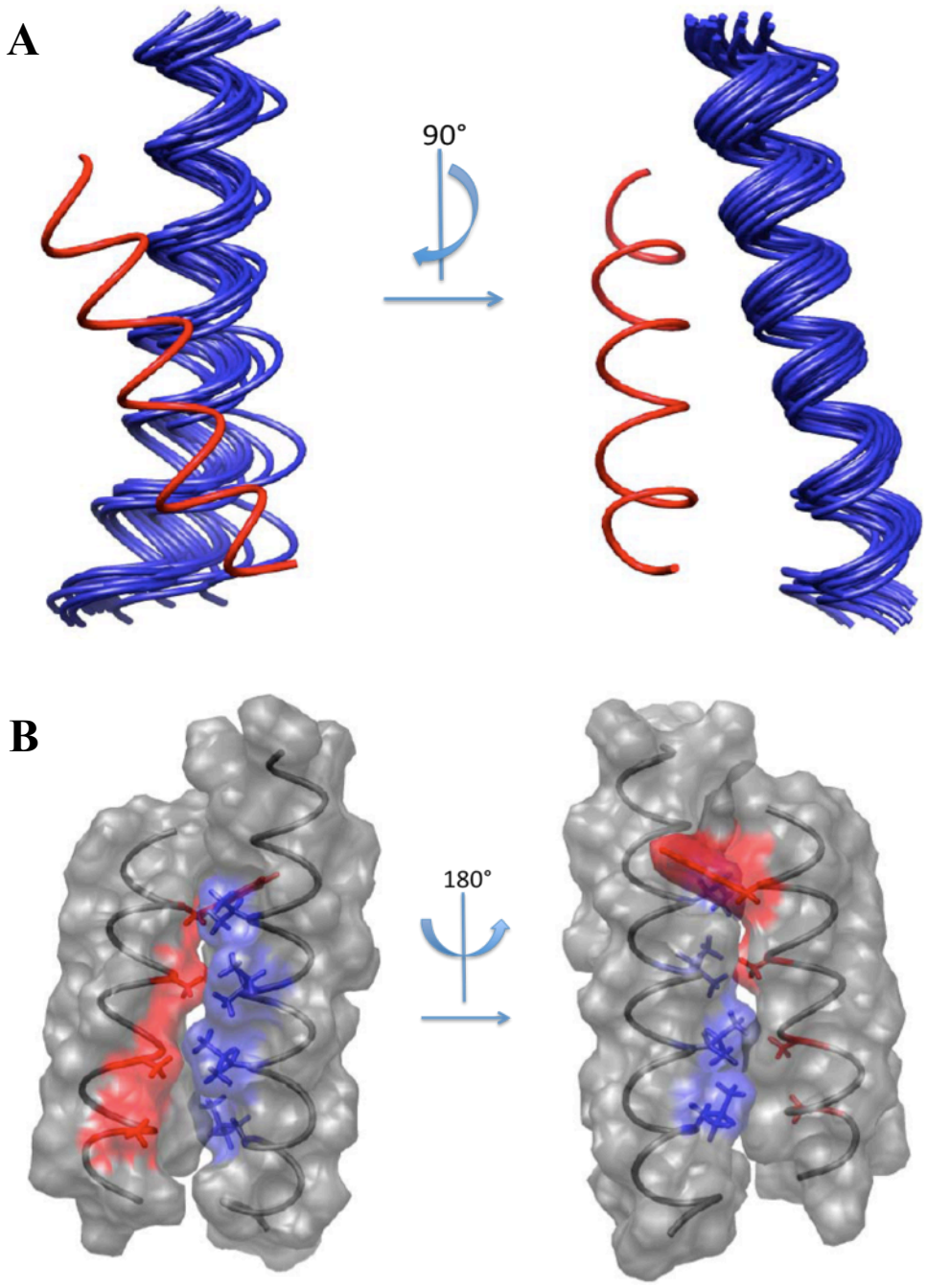

Figure 4.12: Docking simulation of BST-2 Vpu complex. A) 20 lowest energy structure ensemble of the complex with Vpu in red as the reference and BST-2 colored in blue. B) Surface representation of the lowest energy complex with the selective side chains of Vpu colored in red and BST-2 in blue.

shown by the RMSD of about 12Å for the lowest 20 structure ensembles. The high value of RMSD indicates that no energetically favored complex pose is found with the Vpu A3XF mutant. Overall, the results are remarkably congruent with the features of interactions derived from the biological and spectroscopic experiments.

Chapter 4, in part, is a reprint of the material as it appears in the Journal of Biological Chemistry 2011. Skasko, M., Wang, Y., Tian, Y., Tokarev, A., Munguia, J., Ruiz, A., Stephens, E.B., Opella, S.J., and Guatelli, J. The dissertation autor was the co-first author of this paper.

Chapter 5. Conclusion

Membrane proteins present a challenging but highly rewarding area of scientific research. Determining the structure and functions of membrane proteins is crucial for understanding cellular activities, disease mechanisms and drug targets. They are difficult to study mainly because the requirement of lipid environment for the proper folding and functions. NMR is a powerful tool for studying membrane protein since it is able to provide structural and dynamic information for membrane proteins under various lipid environments. Solution NMR can be performed on the protein-micelle complex while solid-state NMR is able to tackle large protein-bicelle or liposome complexes. Solution NMR has relatively quicker experimental setup and higher spectral resolution, but solid-state NMR has the advantage of offering more structural information and a more biological relevant lipid environment. Both techniques can be very complementary to each other when applied to the same protein.

Vpu is a small viral membrane protein from HIV-1 that plays important roles in the virus replication cycle. Using solution NMR, the secondary structures features of various constructs of Vpu are identified with RDC values and q-titration experiments, and they are consist of a single transmembrane helix with two amphipathic surface helices. Comparative study of Vpu and M2 TM domains reveals the dramatic effect of a histidine residue on the tilt angle and proton sensitivity of the transmembrane helix. The histidine increases the tilt angle by around 10°, and enables the transmembrane domain to become sensitive to proton concentration. In addition, by comparing a chimeric M2-Vpu construct with the wildtype Vpu-FL,

we were able to determine that the oligomerization state of Vpu is most likely a tetramer, albeit a less stable one. The dynamics of Vpu, especially the cytoplasmic domain is consistent with the proposed mechanism for its in vivo function. The loop region between the two amphipathic helices is crucial for the β-TrCP recruitment, and its flexibility is a crucial property to maintain its exposure for interaction. This is demonstrated through the 'q-titration' experiment in which the loop was able to maintain almost full-range of motions even when the helical regions were bound to the surface of a bicelle. This is likely due to the numerous charged residues on that region. As for the solid-state results, the 1D spectra of full-length, TM, and cytoplasmic constructs indicate that all of them are strongly associated with the lipids. The 2D spectra indicate that their dynamics are clearly different as TM appears to be the only stable construct within the bicelle environment, and both full length and cytoplasmic constructs have significant motions that cause a dramatic decrease in the spectral resolution. It can be concluded that cytoplasmic domain has certain dynamics that not only affect itself but also the TM domain. Whether this motion occurs in vivo is not known, but it makes a very significant contribution in terms of the NMR acquisition time scale. There are several areas that can be optimized that could potentially resolve this issue. One is the lipid environment which can be varied by changing certain properties such as hydrocarbon chain length and head-group properties. For example, the lipids with zwitterionic head groups can be replaced or supplemented with a negatively or positively charged head group at different concentration so that the cytoplasmic domain can potentially become more stabilized. Different spectroscopic

techniques which also alleviate the problems introduced by the dynamics. One such technique is magic angle spinning (MAS) solid-state NMR which uses a rotor to spin the sample at a particular angle with respect to the magnetic field in order to remove the broadening effect of dipolar coupling. The resulting experimental data consist of isotropic chemical shifts of observed nuclei and the dipolar coupling values can also be obtained through recoupling experiments. These data can then be used for structural characterization. Significant progress is being made on both Vpu-full length and cytoplasmic constructs by other members of Opella group using MAS NMR as this thesis is being written.

Protein-protein interaction is the main functional feature of Vpu which include the well studied CD4 down-regulation and the recent discovery of BST-2 antagonism. The details of either mechanism still have not been elucidated because the results can be difficult to interpret, especially under in-cell biological condition, because of various proteins and cellular environments that can affect the outcomes. Therefore, it is important to study the functional aspects of Vpu at molecular levels so that we can isolate the different biochemical properties of the interaction. Fortunately, NMR is just as powerful as a technique for interaction studies as it is for structure determination because it is able to monitor the interaction induced perturbation of individual residues as well as the overall structure and topology. However, these derived biochemical properties should ultimately be validated in biological experiments to confirm the relevance. In the spirit of mutual benefit, the collaborative studies of the protein-protein interaction between BST-2 and Vpu provided extraordinary insights into a

very complex mechanism. To summarize the important findings, solution NMR experiments revealed important residues of both proteins involved in the interaction, and confirmed the lack of interaction for a Vpu mutant that was found to be defective in biological assays. In addition, a high resolution backbone structure of BST-2 TM domain was able to be obtained from the solution NMR experimental data. Solid-state NMR revealed a tilt angle different between the two proteins and the interaction resulted in changes in tilt angle and dynamics for BST-2 while causing no significant perturbation to Vpu. The difference observed between ΔLG T45I mutant and wildtype of BST-2 in solid-state NMR gives an example of the possible biological relevance of the tilt angle of transmembrane helices in protein-protein interaction.

Further research is needed to get a better understanding of this interaction. In particular, a high-resolution experimentally determined structure of the complex would be very useful for describing the interaction, and intermolecular distance information is required for that accomplishment. This can be particularly challenging considering the fast decay of the intermolecular transfer signal and the exchange effect due to the weak interaction. There are several strategies to overcome the challenges, and one of them is using paramagnetic relaxation enhancement (PRE) since it is a very sensitive experiment with a large effective range. In fact, some progress has already been made using paramagnetic spin-label as shown in the experiment that described the anti-parallel conformation. Average intermolecular distances were able to be obtained from the fitting of the data. Unfortunately, the distances are limited to the unstructured backbone areas that are not part of the transmembrane domains, so it

would be difficult to use them to constrain the complex structure. However, work can be done to attach spin labels towards the center of the TM to obtain more useful structural restraints, and this approach can be applied to both solution and solid-state NMR samples. One caveat is that validation experiments are needed to ensure no extra perturbations are introduced due to the mutation or attachment. In addition to PRE, side-chain intermolecular NOEs can also be used to obtain direct structure information for the complex. As described in the introduction chapter, NOEs are difficult to obtain for membrane proteins because of fast T_2 relaxation, and in the case of protein-protein interaction, the problem is compounded by the chemical exchange factor introduced by the partial dissociation of the complex. This can be alleviated by observing the side-chain nuclei which are expected to be closer in distance in comparison to the backbone signals, and the solution NMR results suggest that several residues become more rigidified upon interaction. This infers that the corresponding side-chains are tightly fitted between the two proteins thus reducing the effect from chemical exchange. These would be good targets to obtain the intermolecular distances for structure calculation. Another difficulty with NOEs, particularly those involving side-chains, is the time consuming resonance assignment process which sometimes produce ambiguous results due to inadequate spectral resolution. One solution to that problem is selectively labeling the side-chains such as methyl carbon labeling which significantly reduces the complexity of the spectrum and the probability of the mis-assignment. This is a common practice for elucidating protein-proteins interactions for large complexes and weak interactions such as protein-DNA/RNA complex.

The overall approach used in characterizing BST-2 and Vpu can be summarized as a combination of ‘top-down’ and ‘bottom up’ research strategies, and can be very effective in describing the mechanism of action in a biological system. The ‘top-down’ refers to taking the results from in-vivo/cellular biological experiments and validating them at molecular or atomic level using biophysical and biochemical methods. The dynamics and interactions at a biological level can have enormous complexity and often difficult to account for all of the variables, so this approach essentially focuses on the behavior of a molecule regarding its most fundamental biochemical level. It also provides insights on whether a finding from the biological experiments is the result of a particular behavior or due to other factors. The ‘bottom-up’ approach refers to deriving the molecular properties/principles from the biophysical or biochemical methods and applying them in biological systems to see if the findings are relevant. This approach is very powerful for building models that describe the behavior of molecules and can give very accurate prediction in the biological outcomes. Both approaches can also have disadvantages. For example, in ‘top-down’, the results from biological experiments may be difficult to be directly tested at a molecular and biophysical level simply due to the sheer complexity of the experimental condition. A specific example would be the extended post-translational modification of a protein that is difficult to duplicate when certain biophysical experiment require the heterologous expression. The ‘bottom-up’ approach often can suffer from the non-biological test condition that gives experiment-specific results that may not directly translate into predictive information for vivo/cellular experiments.

Therefore, there is a need for a combination of the two approaches and continuous feed back and validation between the results generated from the two approaches in order to provide a more accurate description of a biological molecule or system. The study on BST-2 Vpu interaction shows that this 'synergetic' strategy is indeed practical and effective.

As the knowledge continues to expand at a rapid pace for the characterization of membrane protein, there are two main considerations that need to be properly addressed when embarking on such studies. One is the integration of structure and function in the study of the proteins since most of them have functions other than pure structural support. It is valuable to obtain details of the rigid structure as well as the dynamic information during functional states such as catalysis or protein binding. These experiments should be done in parallel, and the information they provide can often be complementary. The other consideration is that it is important to perform these characterizations with the consistency in protein construct, lipid complex and buffer environment, as variables would complicate the interpretation of the combined data. NMR spectroscopy is one the few techniques that offer this rare versatility in characterizing membrane proteins in several kinds of environment, both structurally and functionally. It therefore provides the consistency that is imperative in formulating a 'whole-picture' description for a membrane protein system, and it will continue to be a powerful force in the development of structural biology.

Bibliography

Alia, A., Ganapathy, S., and de Groot, H.J. (2009) *Photosynth. Res.* 102, 415-425.

Battiste, J.L, and Wagner, G. (2000) *Biochemistry*. 39, 5355-5365.

Clore, G.M., Tang, C., and Iwahara, J. (2007) *Biophysical Methods*. 17, 603-616.

Cohen, E.A., Terwilliger, E.F., Sodroski, J.G., and Haseltine, W.A. (1988) *Nature.* 334, 532-534.

Cornilescu, G., Delaglio, F., and Bax, A. (1999) *Journal of Biomolecular NMR*. 13, 289-302.

Deisenhofer, J., Epp, O., Miki, K., Huber R. and Michel H. (1985) *Nature* 318, 618-624.

Delaglio, F, Grzesiek, S., Vuiser, G.W., Zhu, G., Pfeifer, J., and Bax A., (1995) *Journal of Biomolecular NMR*. 6, 277-293.

Dube, M., Bego, M.G., Paquay, C., and Cohen, E.A. (2010) *Retrovirology*. 7:114.

Ewart, G.D., Mills, K., Cox, G.B., and Gage, P.W. (2002) *Eur. Biophys. J*. 31, 26-35.

Grant, C.V., Yang, Y., Glibowicka, M., Wu, C.H., Park, S.H., Deber, C.M., and Opella, S.J. *Journal of Magnetic Resonance.* 201, 87-92.

Gray, J.J., Moughon, S., Wang, C., Schueler-Furman, O., Kuhlman, B., Rohl, C.A., and Baker, D. (2003) *Journal of Molecular Biology*. 331, 281-299.

Grzesiek, S., Dobeli,, H., Gentz, R., Garotta, R., Labhardt,, A.M., and Bax, A. (1992) *Biochemistry*. 31, 8180-8190.

Hout, D.R., Gomez, L.M., Pacyniak, E., Miller, J-M., Hill, S., and Stephens, E.B. (2006) *Virology*. 348, 449-461.

Johnson, B.A., and Blevins, R.A. (1994) *Journal of Biomolecular NMR*. 4, 603-614.

Koradi, R., Billeter, M., and Wuthrich, K. (1996) *J. Mol. Graph*. 14, 51-55.

Kreuger-Koplin, R.D., Soren, P.L, Krueger-Koplin, S.T., Reivera-Torres, I.O., Cahill, S.M., Hicks, D.B., Grinius, L., Krulwich, T.A., and Girvin, M.E. (2004) *Journal of Biomolecular NMR.* 17, 43-57.

Leopold, M.F., Urbauer, J.L., and Wand, A.J. (1994) 2, 61-93.

Lipsitz, R.S., and Tjandra, N. (2004) *Annu. Rev. Biophys. Biomol. Struct.* 33, 387-413.

Ma, C., Marassi, F.M., Jones, D.H., Straus, S.K., Bour, S., Strebel, K., Schubert, U., Oblatt-Montal, M., Montal, M., and Opella, S.J. (2002) *Protein Science*. 11, 546-557.

Marassi, F.M., and Opella S.J. (2000) *Journal of Magnetic Resonance*. 144, 150-155.

McDermott, A. (2009) *Annu. Rev. Biophys.* 38, 385-403.

Mesleh, M.F., and Opella, S.J. (2003) *Journal of Magnetic Resonance*. 163, 288-299.

McNatt, M.W., Zang, T., Hatziioannou, T., Bartlett, M., Fofanna, I.B., Johnson, W.E., Neil, S.J.D., and Bieniasz, P.D. (2009) *PLOS Pathogens*. 5:e1000300.

Muhandiram, D.R., and Kay, L.E. (1994) *Journal of Magnetic Resonance B*. 103, 203-216.

Muller, L., Kumar, A., Baumann, T., and Ernst, R.R. (1974) *Physical Review Letters.* 32, 1402-1406.

Mukhopadhyay, R., Miao, X., Shealy, P., and Valafar, H. (2009) *Journal of Magnetic Resonance.* 198, 236-247.

Neil, S.J., Zang, T., and Bieniasz, P.D. (2008) *Nature* 451, 425-431.

Nevzorov, A.A., and Opella, S.J. (2003) *Journal of Magnetic Resonance*. 164, 182-186.

Nevzorov, A.A., Mesleh, M.F., and Opella, S.J. (2004) Magnetic Resonance in Chemistry. 42, 162-171.

Park, S.H., Mrse, A.A., Nevzorov, A.A., Mesleh, M.F., Oblatt-Montal, M., Montal, M., and Opella S.J. (2003) *Journal of Molecular Biology*. 333, 409-424.

Park, S.H., and Opella, S.J. (2007) *Protein Science*. 16, 2206-2215.

Park, S.H., and Opella, S.J. (2010) *J. Am. Chem. Soc.* 132, 12552-12553.

Perez-Caballero, D., Zang, T., Ebrahimi, A., McNatt, M.W., Gregory, D.A., Johnson, M.C., and Bieniasz, P.D. (2009) *Cell*. 139, 499-511.

Pettersen, E.F., Goddard, T.D., Huang, C.C., Couch, G.S., Greeenblatt, D.M., Meng, E.C., and Ferrin, T.E. (2004) *Journal of Computational Chemistry*. 25, 1605-1612.

Pinto, L.H., and Lamb, R.A. (2006) *Journal of Biological Chemistry*. 281, 8997-9000.

Planque, M.R.R., Bonev, B.B., Demmers, J.A.A., Greathouse, D.V., Koeppe, R.E., Separovic, F., Watts, A., and Killian,, J.A. (2003) *Biochemistry.* 42, 5341-5348.

Schramm, S., and Oldfield E. (1983) *Biochemistry* 22, 2908-2913.

Staley, J., and Kim, P. (1994) *Protein Science*. 3, 1822-1832.

Schwieters, C.D., Kuszewski, J.J., Tjandra, N., Clore, G.M. (2002) *Journal of Magnetic Resonance*. 160, 65-73.

Schnell, J.R., and Chou, J.J. (2008) *Nature*. 451, 591-596.

Senes, A., Engel, D.E., and DeGrado, W.F. (2004) *Current Opinion in Structural Biology*. 14, 465-479.

Sharma, M., Yi, M., Dong, H., Qin, H., Peterson, E., Busath, D.D., Zhou, H-X., and Cross, T.A. (2010) *Science*. 330, 509-512.

Stouffer, A.L., Nanda, V., Lear, J.D., and DeGrado, W.F. (2005) *Journal of Molecular Biology*. 347, 169-179.

Stouffer, A.L., Acharya, R., Salom, D., Levine, A.S. Costanzo, L.D., Soto, C.S., Terehko, V., Nanda, V., Stayrood, S., and DeGrado, W.F. (2008) *Nature*. 451, 596-600.

Tang, Y., Zaitsev F., Lamb, R.A., and Pinto, L.H. (2002) *Journal of Biological Chemistry.* 277, 39880-39886.

Van Damme, N., Goff, D., Katsura, C., Jorgenson, R.L., Mitchell, R., Johnson, M.C., Stephens, E.B., and Guatelli, J. (2008) *Cell Host & Microbe*. 3, 245-252.

Venkataraman, P., Lamb, R.A., and Pinto, L.H. (2005) *Journal of Biological Chemistry.* 280, 21463-21472.

Wang, K., Xie, S., and Sun, B. (2011) *Biochim. Biophys. Acta*. 2,510-515.

Whiles, J.A., Deems, R., Vold, R.R., and Dennis, E.A. (2002) *Bioorganic Chemistry* 30, 431-442

Whitehead, B., Craven, C.J., and Waltho, J.P. (1997) *Methods. Mol. Biol.* 60, 29-52.

Wildum, S., Schindler, M., Munch, J., and Kirchhoff. (2006) *Journal of Virology.* 80, 8047-8059.

Willbold, D., Hoffmann, S., and Rosch, P. (1997) *Eur. J. Biochem*. 245, 581-588.

Wishart, D.S., and Sykes, B.D. (1994) *Journal of Biomolecular NMR*. 4, 171-80.

Wittlich, M., Koenig, B.W., Stoldt, M., Schmidt, H., and Willbold, D. (2009) *The FEBES Journal*. 276, 6560-6575.

Wu, C.H., Grant, C.V., Cook, G.A., Park, S.H., and Opella, S.J. (2009) *Journal of Magnetic Resonance.* 200, 74-80.

Yang, H., Wang, J., Jia, X., McNatt, M.W., Zang, T., Pan, B., Meng, W., Wang, H., Bieniasz, P.D., and Xiong, Y. (2010) *PNAS*. 107, 18428-18432.